HIGH CROSSOVER RATE1 encodes PROTEIN PHOSPHATASE X1 and restricts meiotic crossovers in Arabidopsis

Divyashree C. Nageswaran[1§], Jaeil Kim[2§], Christophe Lambing[1], Juhyun Kim[2], Jihye Park[2], Eun-Jung Kim[2], Hyun Seob Cho[2], Heejin Kim[2], Dohwan Byun[2], Yeong Mi Park[2], Pallas Kuo[1], Seungchul Lee[2], Andrew J. Tock[1], Xiaohui Zhao[1], Ildoo Hwang[2], Kyuha Choi[1,2,*] and Ian R. Henderson[1,*]

[1] Department of Plant Sciences, Downing Street, University of Cambridge, Cambridge, CB2 3EA, United Kingdom
[2] Department of Life Sciences, Pohang University of Science and Technology, Pohang, Gyeongbuk, Republic of Korea

§ Equal contribution

* Correspondence: kyuha@postech.ac.kr and irh25@cam.ac.uk

Abstract

Meiotic crossovers are tightly restricted in most eukaryotes, despite an excess of initiating DNA double-strand breaks. The majority of plant crossovers are dependent on Class I interfering repair, with a minority formed via the Class II pathway. Class II repair is limited by anti-recombination pathways, however similar pathways repressing Class I crossovers are unknown. We performed a forward genetic screen in Arabidopsis using fluorescent crossover reporters, to identify mutants with increased or decreased recombination frequency. We identified *HIGH CROSSOVER RATE1* (*HCR1*) as repressing crossovers and encoding PROTEIN PHOSPHATASE X1. Genome-wide analysis showed that *hcr1* crossovers are increased in the distal chromosome arms. MLH1 foci significantly increase in *hcr1* and crossover interference decreases, demonstrating an effect on Class I repair. Consistently, yeast two-hybrid and *in planta* assays show interaction between HCR1 and Class I proteins, including HEI10, PTD, MSH5, and MLH1. We propose that HCR1 plays a major role in opposition to pro-recombination kinases to restrict crossovers in Arabidopsis.

Keywords: Meiosis, crossover, interference, phosphatase, PPX1, PP4, Arabidopsis.

Main text

Meiosis is a specialized cell division occurring in eukaryotes, where a single round of DNA replication is coupled to two rounds of chromosome segregation, to generate haploid cells that can undergo sexual fusion[1,2]. During meiotic prophase I, homologous chromosomes pair and undergo programmed recombination, which can produce reciprocal crossovers between chromosomes[1,2]. Meiotic recombination and chromosome segregation cause the haploid gametes to be genetically mosaic[1,2]. As a consequence, sex has a profound effect on genetic variation and adaptation[1,2].

Meiotic recombination initiates with formation of DNA double strand breaks (DSBs), via a conserved topoisomerase-related protein SPO11[1,2]. In plants, SPO11-1 and SPO11-2 form a heterotetramer with MTOPVIB to generate meiotic DSBs[3–5]. Mutation of *spo11-1*, *spo11-2* or *mtopvib* prevents homolog pairing, causing univalent segregation at metaphase I and aneuploid gametes in Arabidopsis[3–5]. Meiotic DSBs are resected to generate single-stranded DNA (ssDNA) that is bound by the RecA-related proteins DMC1 and RAD51[6]. DMC1/RAD51 nucleofilaments mediate interhomolog strand invasion to form displacement loops[2,6]. In wild type Arabidopsis, ~150-250 DSB-associated foci are evident along the meiotic chromosome

axis, when DMC1, RAD51, RPA1a and γH2A.X are immunostained during early meiotic prophase I[2,7]. In wild type Arabidopsis, only ~10 of these DSBs are ultimately repaired as interhomolog crossovers[2,8]. The remaining strand invasion events are disassembled by non-crossover pathways, which include FANCM, RECQ4A, RECQ4B and FIGL1[2,9]. Meiotic DSBs may also be repaired using the sister chromatid[2,10].

In plants, the major pathway generating crossovers is termed Class I (also known as the ZMM pathway)[2]. Class I crossovers show interference, meaning they are more widely spaced than expected by chance[11]. In plants, ~80-85% of crossovers are dependent on the Class I pathway, which includes *MSH4*, *MSH5*, *ZIP4*, *SHOC1*, *PTD*, *HEI10*, *HEIP1*, *MER3*, *MLH1* and *MLH3*[2,12]. The Class I pathway functions to stabilize interhomolog joint molecules and promotes crossover resolution via double Holliday junctions[13]. Within this pathway; MSH4 and MSH5 form the MutSy heterodimer that associates with meiotic chromosomes and stabilizes interhomolog joint molecules[13], SHOC1 and PTD form a catalytically inactive XPF:ERCC1 endonuclease-related complex that has affinity for joint molecules[13], HEI10 belongs to a family of ubiquitin and SUMO E3 ligases[13], MER3 is a DNA helicase[14], and MLH1 and MLH3 form the MutLy heterodimer, which has endonuclease activity[13]. A minority (~15-20%) of crossovers in plants are non-interfering and dependent on the Class II pathway[2]. In anti-recombination pathway mutants, for example *recq4a recq4b*, large increases in Class II crossovers occur[15,16].

Progression of the meiotic cell cycle and recombination are regulated by multiple protein kinases pathways, whose targets include DSB proteins, the Class I pathway and the chromosome axis[17]. For example, cell division kinase CDK1;A promotes Class I crossovers in Arabidopsis, and directly targets MLH1 *in vitro*[18]. In mammals and budding yeast, the ATM/ATR (Mec1/Tel1) DNA damage kinases are activated by meiotic DSBs, and mediate feedback signalling on recombination in *cis* and *trans*[19–21]. Zip3, the budding yeast HEI10 ortholog has been shown to be an Mec1/Tel1 target in budding yeast[22], which is antagonized by the PPH3 PP4 protein phosphatase complex[22]. The Dbf4/Drf1-dependent kinase Cdc7 complex (DDK) phosphorylates a MSH4 degron to stabilize its association with recombination sites in budding yeast[23]. Proteins of the chromosomes axis, including ASY1 and REC8, are also extensively phosphorylated during meiosis[24,25]. How protein kinases and phosphatases are balanced to control meiotic crossovers in plants remains unknown.

To identify new factors that control meiotic recombination we performed a forward genetic screen using a fluorescent crossover reporter. This screen identified the *high crossover rate1* (*hcr1*) mutant in *PROTEIN PHOSPHATASE X1*, which functions in the nuclear PP4 protein phosphatase complex[26–28]. Crossovers increased most strongly in distal euchromatic regions in *hcr1* and the strength of interference decreased. As MLH1 foci significantly increase in *hcr1*, this shows that HCR1 represses the Class I crossover pathway. Consistently, yeast two-hybrid and co-immunoprecipitation assays show that HCR1 interacts with the Class I proteins HEI10, PTD, MSH5 and MLH1. We also observed two-hybrid interactions between HCR1 and chromosome axis proteins, DSB factors and recombinases, indicating a potential broader regulatory role during meiosis. We propose that HCR1/PPX1 PP4 phosphatases act in opposition to pro-recombination kinase pathways, in order to limit crossovers in Arabidopsis.

Results

A forward genetic screen for mutants with altered meiotic crossover frequency

To isolate new factors controlling meiotic crossover frequency we performed a forward genetic screen in *Arabidopsis thaliana* (Fig. 1a). Fluorescent reporters of crossover frequency are available in Arabidopsis, which consist of linked FTL/CTL T-DNA insertions expressing different colors of fluorescent protein in the seed (*NapA* promoter) or pollen (*LAT52* promoter)[29–31] (Fig. 1b). When FTLs are hemizygous, inheritance of fluorescence can be used

to score crossover frequency within the interval defined by the T-DNAs[29–32] (Fig. 1b). We selected the *420* FTL for mutagenesis, which defines a 5.1 megabase interval located in the left sub-telomeric region of chromosome 3[30,32] (Fig. 1a,b). *420* was chosen for mutagenesis, as crossover frequency in this region is known to be sensitive to multiple recombination and chromatin pathways[32–36].

We generated ~10,000 *420/*++ hemizygous seed via crossing and used this for ethyl methanesulfonate (EMS) mutagenesis (Fig. 1a). From these seed, ~7,000 M_1 plants were grown and M_2 seed was collected (Fig. 1a). The seed from 12 independent M_1 plants were combined to generate ~600 M_2 pools (Fig. 1a), and seed within these pools were pre-selected to be red-green fluorescent (*420/*++ hemizygous). Approximately 150 pre-selected seeds were grown from each M_2 pool and allowed to self-fertilize (Fig. 1a). Seed from individual M_2 plants were used to score crossover frequency within *420* (Fig. 1a,b). In our growth conditions, *420* in self-fertilized wild type Col/Col inbred plants shows a mean crossover frequency of 20.19 cM (standard deviation=1.43) (Fig. 1c and Table S1). In total, 2,883 M_2 individuals were screened and the majority (81.4%) showed *420* crossover frequency within the range of 18-22 cM (Extended Data Fig. 1). 19 putative high or low crossover frequency mutants were self-fertilized and M_3 progeny tested for *420* crossover frequency, of which 5 were confirmed to show a heritable recombination phenotype in the next generation (Fig. 1a).

We identified four mutants with high and one with low *420* crossover frequency (Fig. 1c and Supplementary Table 1), which we term *high crossover rate1* (*hcr1*), *hcr2*, *hcr3*, *hcr4* and *low crossover rate1* (*lcr1*). The *hcr4* mutant was shown to be allelic to *fancm* (Extended Data Fig. 2 and Supplementary Table 1), which is a known repressor of Class II crossovers[37]. The *hcr4* (*fancm-11*) allele is caused by a non-synonymous amino acid substitution (G540S) in the conserved SF2 helicase domain and shows a comparable effect on *420* crossover frequency to the *fancm-1* allele[37] (Fig. 1c, Supplementary Table 1 and Extended Data Fig. 2). We identified that *lcr1* was allelic with the *taf4b* mutant (*taf4b-3*) (Supplementary Table 2 and Extended Data Fig. 2), which was previously shown to promote crossovers in the distal chromosome arms[34]. In this study we focused on identification and functional characterization of *hcr1* (Fig. 1c).

To map the *hcr1* mutation we produced a BC_1F_2 mapping population by backcrossing M_3 *hcr1 420* (*GR/GR*) plants to wild type (Col) (Fig. 1a and Fig. 2a). *420* crossover frequency was not significantly different between *hcr1/*+ BC_1F_1 and wild type, showing that *hcr1* is recessive (Welch's t-test, P=0.241) (Fig. 2a and Supplementary Table 3). The *hcr1/*+ *420/*++ BC_1 hybrid plants were then self-fertilized to generate a 300 individual BC_1F_2 population, which were scored for *420* crossover frequency (Fig. 1a). Material from the 60 BC_1F_2 plants with highest *420* crossover frequency was pooled and used for genomic DNA extraction and short-read sequencing (Fig. 2a). We applied the SHORE[38] mapping pipeline in order to identify candidate EMS mutations in the high crossover BC_1F_2 sequencing library (Fig. 2b). The candidate mutation with highest frequency was a G to A substitution in a splice donor site of the 3rd intron of At4g26720, which encodes PROTEIN PHOSPHATASE X1 (PPX1)[28] (Fig. 2b,c and Supplementary Table 4).

HIGH CROSSOVER RATE1 encodes PROTEIN PHOSPHATASE X1

We used RT-PCR to amplify and sequence *PPX1* mRNA from *hcr1* plants, which revealed intron 3 retention, causing a premature stop codon (Fig. 2c and Extended Data Fig. 3). The stop codon is predicted to truncate PPX1 (143 of 305 residues) and remove conserved metal-binding histidine residues in the C-terminal region[39] (Fig. 2c and Extended Data Fig. 4a). However, the truncated protein has the potential to encode three of four conserved PPX1 catalytic motifs (GDXHG, GDXVDRG and GNHE) in the N-terminal region[39] (Fig. 2C and Extended Data Fig. 4a). PPX1 is the catalytic subunit of the hetero-multimeric PP4

serine/threonine protein phosphatase complex, which includes two additional regulatory subunits (PP4R2 and PP4R3)[40] (Fig. 2d). PP4 complexes have multiple roles in mitotic and meiotic DNA recombination and repair in diverse eukaryotes[26,41–49].

To prove whether the splice acceptor mutation in *PPX1* causes the *hcr1 420* crossover phenotype, we performed a complementation test (Fig. 2f and Supplementary Table 5). A 4,515 bp genomic fragment containing the *PPX1* gene was PCR amplified from wild type (Col) and inserted into an Agrobacterium binary vector and used to transform *hcr1 420/++* plants. We observed that the *hcr1* plants transformed with *PPX1*, but not empty vector, showed *420* crossover frequency not significantly different to wild type (Welch's t-test, P=0.357) (Fig. 2f and Supplementary Table 5). We obtained a second T-DNA insertion (GK_651B07) mutation in *PPX1*, using a located in the 5′-UTR, which we term *hcr1-2*, and term the EMS allele *hcr1-1* (Fig. 2c,g and Supplementary Table 6). We measured *420* crossover frequency in *hcr1-2* homozygotes and observed a significant increase compared to wild type (Welch's t-test, $P=5.43\times10^{-8}$) (Fig. 2g and Supplementary Table 6), although the phenotype was weaker than *hcr1-1*. We crossed *hcr1-1* with *hcr1-2* to generate *hcr1-1/hcr1-2* F_1 hybrids, which showed significantly higher *420* crossovers compared to wild type, demonstrating allelism (Welch's t-test, $P=4.91\times10^{-10}$) (Fig. 2g and Supplementary Table 6). Together, these genetic data identify *PPX1* as *HCR1*.

The Arabidopsis genome encodes a second PP4C catalytic subunit gene *PPX2* (At5g55260) which shows 93.8% amino acid sequence identity to PPX1[50–52] (Fig. 2d and Extended Data Fig.4). Functional redundancy between Arabidopsis *PPX1* and *PPX2* has been observed previously[28]. We obtained a T-DNA insertion in *PPX2* (GK_488H09), which disrupts mRNA expression, but did not observe a significant effect on *420* crossovers, compared to wild type (Welch's t-test, P=0.119) (Fig. 2h, Extended Data Fig. 3a,b and Supplementary Table 7). However, *hcr1-2 ppx2-1* double mutants showed a significant increase in *420* crossovers, compared to *hcr1-2* (Welch's t-test, $P=1.42\times10^{-4}$) (Fig. 2h and Supplementary Table 7). We also crossed *hcr1-1* with a second *ppx2* T-DNA insertion allele (*ppx2-2*) and failed to identify *hcr1-1 ppx2-2* double mutants in the F_2 generation. As the siliques of *hcr1-1/+ ppx2-2/+* plants contained aborted seed not seen in wild type controls, this supports that the double mutant is embryo or seedling lethal (Extended Data Fig. 3d-3f). Arabidopsis encodes a single gene for the PP4R2 regulatory subunit (At1g17070), and we obtained a T-DNA insertion that disrupts mRNA expression of this gene (Extended Data Fig. 3a,b). We observed that *pp4r2* shows a significant increase in *420* crossover frequency, compared to wild type (Welch's t-test, $P=4.24\times10^{-5}$), with a similar phenotypic strength to *hcr1-2* (Fig. 2h and Supplementary Table 7). As *pp4r2* mutants are viable, this indicates that the T-DNA insertion is likely to be hypomorphic. Together, this is consistent with HCR1/PPX1 and PPX2 acting in PP4 complexes with PP4R2 to repress meiotic crossovers in Arabidopsis. We also note that recent mass spectroscopy data from Arabidopsis has confirmed the presence of HCR1/PPX1, PPX2, PP4R2L and PP4R3A complexes *in vivo*[28].

Meiosis-specific knockdown of *HCR1/PPX1* and *PPX2* using meiMIGS

Our genetic analysis indicates functional redundancy between *PPX1* and *PPX2* (Fig. 2h). This is consistent with null *ppx1 ppx2* double mutants causing severe developmental phenotypes, not observed in the single mutants[28]. Therefore, we sought to silence both *PPX1* and *PPX2* specifically during meiosis. For this purpose we adapted miRNA-induced gene silencing (MIGS) for use during meiosis[53]. MIGS constructs fuse a microRNA173 (miR173) target site upstream of target transcript sequences[53]. Transcript cleavage of the fusion RNA by endogenous miR173 is an efficient trigger of 22 nucleotide trans-acting siRNAs (tasiRNAs), which act to silence endogenous gene transcripts that share sequence homology in *trans*[53]. To drive MIGS specifically during meiosis (meiMIGS), we expressed miRNA173-target *PPX1* and *PPX2* gene fusions from the *DMC1* promoter[54] (Fig. 3a). We measured *PPX1* and *PPX2*

transcripts levels from meiotic stage floral buds in meiMIGS transformed plants and observed a significant reduction of both genes in all tested lines, compared to wild type (Welch's t-test, all $P<1.51\times10^{-9}$) (Extended Data Fig. 5). Cross-silencing of *PPX1* and *PPX2* by the meiMIGS constructs is expected, as these genes share 86.6% nucleotide identity. The constructs were transformed into *420*/++ plants and we observed a significant increase in crossover frequency compared to wild type (Welch's t-test, all $P<1.01\times10^{-4}$) (Fig. 3b and Supplementary Table 8). We correlated relative expression of *PPX1* and *PPX2* in these backgrounds with *420* crossover frequency and observed a significant negative correlation in both cases (*PPX1* r=-0.76 $P=6.73\times10^{-5}$, *PPX2* r=-0.64 $P=1.81\times10^{-3}$) (Fig. 3b-3c and Extended Data Fig. 5). Together, this demonstrates quantitative increases in crossover frequency that correlate with the degree of *PPX1* and *PPX2* silencing.

Euchromatic crossovers increase and the strength of interference decreases in *hcr1* and *meiMIGS-PPX1-PPX2*

To investigate the effect of *hcr1* and *meiMIGS-PPX1-PPX2* on crossover frequency in other genomic regions, we crossed these lines with additional FTL/CTL recombination reporters[29–31] (Fig. 3d), expressing fluorescent proteins using either seed (Fig. 3e,f), or pollen promoters (Fig. 3g). Plants carrying seed-based CTL reporters were self-fertilized and measure both male and female meiosis (Fig. 3e,f). We observed that distal FTL intervals *CTL1.17, CTL1.26*, *CTL3.15* and *CTL5.4* showed significantly higher crossover frequency in *hcr1-1*, compared to wild type (Welch's t-test, all $P<1.08\times10^{-4}$) (Fig. 3e and Supplementary Table 9). In contrast, the centromere spanning interval *CTL5.11* did not significantly change in *hcr1-1* (Fig. 3e and Supplementary Table 9). The same patterns were confirmed using *meiMIGS-PPX1-PPX2*, which showed significant crossover increases in the distal and interstitial FTL intervals *CTL1.13, CTL1.22, CTL2.2, CTL2.7, CTL4.7, CTL5.1* and *CTL5.13*, compared to wild type (Welch's t-test, all $P<1.71\times10^{-3}$), whereas the centromeric interval *CTL5.5* did not significantly change (Fig. 3f and Supplementary Table 10).

We crossed *meiMIGS-PPX1-PPX2* with pollen-based FTL intervals, which are combined with the *quartet1* mutation[31] (Fig. 3d, 3g,h and Supplementary Table 11-12). This assay measures crossover frequency and interference specifically in male meiosis[31]. For analysis we used a deep learning pipeline DeepTetrad, which enables high-throughput analysis of fluorescent tetrads[55]. We tested four three-color FTL intervals located in distal chromosome regions; *I1bc*, *I1fg*, *I3bc* and *I5ab*. All intervals, except the relatively narrow *I1g*, showed significant crossover increases in *meiMIGS-PPX1-PPX2* compared to wild type (Welch's t-test, all $P<7.28\times10^{-3}$) (Fig. 3g, Extended Data Fig. 6 and Supplementary Table 11). We also tested the centromere-spanning FTL *CEN3*, which significantly decreased in *meiMIGS-PPX1-PPX2* (Welch's t-test, $P=5.05\times10^{-3}$) (Fig. 3g and Supplementary Table 12). Across all FTL data, we correlated the proximity of each interval midpoint to the centromere, with the change in crossover frequency that occurred in *hcr1-1* or *meiMIGS-PPX1-PPX2* relative to wild type (Fig. 3i and Supplementary Tables 9-12). This analysis revealed a significant negative correlation (r=-0.709 $P=1.48\times10^{-4}$) between the crossover increase and proximity to the centromere (Fig. 3i). These results show that the distal chromosome regions significantly increase crossovers in *hcr1* and *meiMIGS-PPX1-PPX2* when measured in male meiosis alone, or in both male and female meiosis. To specifically compare male and female recombination, we backcrossed wild type, *hcr1* and *meiMIGS-PPX1-PPX2* plants that were *420/*++ hemizygous, as either male or female parents. The *420* interval is heterochiasmic and shows significantly higher crossover frequency in male (24.23 cM), compared with female (10.98 cM) (Welch's t-test $P=2.92\text{x}10^{-6}$) (Figure 3j and Supplementary Table 13). We observed that both *hcr1* and *meiMIGS-PPX1-PPX2* showed significant crossover increases in male (Welch's t-test $P=6.25\times10^{-7}$ and 2.15×10^{-7}) and female (Welch's t-test $P=2.81\times10^{-3}$ and 1.75×10^{-3}) meiosis, compared to wild type (Figure 3j and Supplementary Table 13).

For three-color, pollen-based FTL intervals we are able to measure crossovers in adjacent regions and thereby measure interference[31,55]. (Fig. 3h, Extended Data Fig. 6b and Supplementary Table 14). Crossover interference ratios (IFR) are calculated using the genetic map distance in the test interval, with and without a crossover occurring in the adjacent interval. An IFR of 1 indicates an absence of interference[31,55]. We observed that *meiMIGS-PPX1-PPX2* causes an increase in crossover frequency, but a decrease in the strength of interference in FTLs *I1bc, I1fg, I3bc* and *I5ab* (Welch's t-test, all $P<3.05\times10^{-3}$) (Fig. 3g,h and Supplementary Table 14). Therefore, a higher incidence of double crossovers in adjacent intervals occurs in *meiMIGS-PPX1-PPX2*, compared to wild type (Extended Data Fig. 6d). We repeated three-color analysis using FTL intervals *I1bc* and *I3bc* in *hcr1-1* and again observed significantly increased crossover frequency and decreased crossover interference (higher IFR) (Welch's t-tests, $P=2.7\times10^{-4}$, $P=8.1\times10^{-3}$) (Extended Data Fig. 6a-c and Supplementary Table 14).

Genome-wide mapping of crossovers in *meiMIGS-PPX1-PPX2*

Our FTL data indicate that the euchromatic chromosome arms undergo an increase in crossover frequency in *hcr1* and *meiMIGS-PPX1-PPX2*. Notably, these FTL experiments were performed in a Col/Col inbred background. Therefore, we sought to test the effect of *meiMIGS-PPX1-PPX2* on crossovers in a hybrid background (Fig. 4a). We crossed wild type (Col), or a *meiMIGS-PPX1-PPX2* transgenic line in the Col background carrying the *420* FTL, to Ler and generated Col/Ler F_1 hybrids (Fig. 4a and Supplementary Table 15). We measured *420* crossover frequency in wild type and *meiMIGS-PPX1-PPX2* Col/Ler F_1 hybrids and observed a significant increase in *meiMIGS-PPX1-PPX2* (Welch's t-test, $P=6.55\times10^{-11}$) (Fig. 4b and Supplementary Table 15). This demonstrates that *PPX1* and *PPX2* repress crossovers in both inbred and hybrid backgrounds.

We self-fertilized wild type and *meiMIGS-PPX1-PPX2* Col/Ler F_1 plants and generated 144 wild type and 192 *meiMIGS-PPX1-PPX2* F_2 plants, from which genomic DNA was extracted. This DNA was sequenced and data was analysed using the TIGER pipeline[8,56], in order to identify crossover locations in each wild type and *meiMIGS-PPX1-PPX2* F_2 individual (Fig. 4a, c-f). Crossovers were mapped to an average of 962 bp and 936 bp in wild type and *meiMIGS-PPX1-PPX2* F_2 populations, respectively (Supplementary Table 15). We observed a significant increase in crossovers per F_2 from 7.86 in wild type, to 8.57 in *meiMIGS-PPX1-PPX2* (Welch's t-test, $P=7.7\times10^{-3}$) (Fig. 4c). We observed increased crossover numbers on each chromosome in *meiMIGS-PPX1-PPX2* compared to wild type (Fig. 4d), and a positive correlation between crossover number and chromosome length (wild type $r=0.986$, *meiMIGS-PPX1-PPX2* $r=0.983$) (Fig. 4d and Supplementary Table 16).

We analysed the crossover landscape in wild type and *meiMIGS-PPX1-PPX2* (Fig. 4e,f). We averaged all chromosome arms along their telomere-centromere axes and plotted crossover frequency per F_2 in wild type and *meiMIGS-PPX1-PPX2* (Fig. 4e,f). Wild type and *meiMIGS-PPX1-PPX2* show a U-shaped distribution of crossover frequency along the chromosomes, with high recombination in the distal sub-telomeres and pericentromeres (Fig. 4e,f). We observed that the first 60-70% of the chromosome arms from the telomeres showed elevated crossovers in *meiMIGS-PPX1-PPX2* compared to wild type, whereas the pericentromeres and centromeres showed a similar level of recombination (Fig. 4e,f), which is consistent with our previous FTL analysis (Fig. 3d-g and 3i). DNA methylation is highest in the centromeric region[33], where recombination is suppressed in both wild type and *meiMIGS-PPX1-PPX2* (Fig. 4e,f). We compared crossover frequency to Col/Ler SNP frequency, which follows an ascending gradient from the telomeres to the centromeres (Fig. 4e,f). The distal regions of the chromosomes with lowest SNP density and lowest DNA methylation underwent the greatest crossover increase in *meiMIGS-PPX1-PPX2*,s compared to wild type (Fig. 4e,f). We analysed nucleosome occupancy (MNase-seq) and SPO11-1-oligos (a marker of meiotic DSBs) around

crossover locations in wild type and *meiMIGS-PPX1-PPX2*, compared to the same number of randomly chosen locations[57,58]. We observed that crossovers in both genotypes showed a similar depletion of nucleosome occupancy and enrichment of SPO11-1-oligos, compared to random positions (Extended Data Fig. 7). This indicates that while distal regions increase crossovers in *meiMIGS-PPX1-PPX2*, recombination retains a local bias for accessible DNA that experiences higher DSB levels.

hcr1 and *meiMIGS-PPX1-PPX2* show elevated Class I MLH1 foci at diakinesis stage

We used cytological analysis to analyze meiosis in *hcr1-1* compared to wild type. We spread wild type and *hcr1-1* male meiocytes and stained chromosomes using 4',6-diamidino-2-phenylindole (DAPI) (Fig. 5a). We observed normal chromosome morphology during prophase I (leptotene and pachytene) in *hcr1-1*, normal bivalent morphology at metaphase I and chromosome segregation during anaphase I and meiosis II (Fig. 5a). This is consistent with *hcr1-1* showing no difference in fertility compared to wild type (Supplementary Table 16). To investigate formation of the chromosome axis and homolog synapsis, we immunostained wild type and *hcr1-1* meiocytes for the HORMA domain protein ASY1 and the synaptonemal complex protein ZYP1, during prophase I (Fig. 5b). Wild type and *hcr1-1* showed normal homolog synapsis and immunostaining of ASY1 and ZYP1 (Fig. 5b).

We immunostained meiocytes in early prophase I for ASY1 and the DSB marker RAD51 and observed no significant difference in RAD51 foci number between wild type and *hcr1-1* (Fig. 5c,d and Supplementary Table 18) (Wilcoxon t-test, P=0.32). This is consistent with normal levels of meiotic DSBs forming in *hcr1* relative to wild type. Finally, we immunostained for the MLH1 Class I protein at diakinesis stage on DAPI-stained male meiocyte spreads (Fig. 5e,f and Supplementary Table 19). Quantification of MLH1 foci numbers per nucleus showed a significant increase in *hcr1-1* (mean=12.1 foci), compared to wild type (mean=10.4 foci) (Wilcoxon test, $P=5.3\times10^{-7}$) (Fig. 5e,f and Supplementary Table 19). We also measured MLH1 foci in wild type (Col) and *meiMIGS-PPX1-PPX2*, using the same transgenic line as for genotyping-by-sequencing. We observed that *meiMIGS-PPX1-PPX2* showed significantly higher MLH1 foci (mean=12.8), compared to wild type (mean=10.7) (Wilcoxon test $P=2.5\times10^{-6}$) (Supplementary Table 20). Together, this is consistent with the crossover increases observed in *hcr1* and *meiMIGS-PPX1-PPX2* being mediated mainly via the Class I repair pathway.

HCR1 interacts with the Class I crossover pathway proteins HEI10, PTD, MSH5 and MLH1

As we observed elevated MLH1 foci in *hcr1* and *meiMIGS-PPX1-PPX2* (Fig. 5e,f), we sought to investigate genetic interactions with the Class I and Class II repair pathways. Class I pathway mutants, for example *zip4*, have low fertility due to reduced crossovers, unbalanced chromosome segregation and aneuploid gametes[14] (Fig. 5a). Fertility of Class I mutants can be restored by mutations that block non-crossover formation and increase Class II crossovers, for example *fancm*[37]. We generated *zip4 hcr1* double mutants and observed that fertility was not restored (Fig. 6a). We performed meiotic chromosome spreads and counted chiasma, bivalents and univalents in wild type (Col), *zip4* and *zip4 hcr1* (Supplementary Table 21). We observed that *zip4* and *zip4 hcr1* showed strongly reduced bivalents (*zip4* mean=0.8, *zip4 hcr1* mean=1.3), compared to wild type (mean=5) (Wilcoxon test, Col vs *zip4* $P=5.22\times10^{-12}$, Col vs *zip4 hcr1* $P=1.43\times10^{-11}$). The bivalent counts for *zip4* and *zip4 hcr1* were not significantly different from one another (Wilcoxon test P=0.11). This is further consistent with a major effect for *hcr1* on the Class I pathway. We also generated *hcr1 fancm* double mutants carrying the *420* FTL interval, and observed an additive increase in genetic distance in the double mutant compared to *hcr1* and *fancm* single mutants (Welch's t-tests, $P=2.7\times10^{-11}$, $P=6.77\times10^{-6}$) (Fig. 6b and Supplementary Table 20). The *hcr1 fancm zip4* triple mutant

showed lower *420* crossover frequency than *hcr1 fancm*, but higher than *fancm zip4* (Welch's t-test, P=5.60×10^{-4}, P=9.93×10^{-4}) (Fig. 6b and Supplementary Table 22). This suggests that *hcr1* may also increase the number of Class II crossovers, at least in a *fancm zip4* mutant background (Fig. 6b and Supplementary Table 22).

We investigated whether HCR1 physically interacts with known components of the meiotic recombination pathways. We cloned HCR1/PPX1 into yeast 2-hybrid (Y2H) AD and BD vectors and tested interactions with Class I proteins, in addition to the PP4 regulatory subunits PP4R2L and PP4R3A (Fig. 6c,d, Extended Data Fig. 8 and Supplementary Table 23). As expected[28], HCR1 interacts strongly with the PP4 regulatory subunits PP4R2L and PP4R3A (Fig. 6c and Supplementary Table 23). Of the tested Class I combinations we observed strong Y2H interactions between HCR1 and HEI10, MSH5 and PTD (Fig. 6c,d). We also detected weaker interactions between HCR1 and the Class I pathway proteins MER3, ZIP4, SHOC1 and MLH1 (Extended Data Fig. 8d and Supplementary Table 22). Within the Class I pathway we observed strong interactions between HEI10, HEIP1 and MSH5, and between SHOC1 and PTD (Extended Data Fig. 8a,b), consistent with data in rice and Arabidopsis[12,59,60]. We additionally tested a wider set of 13 meiotic proteins that included the synaptonemal complex protein ZYP1a, DNA repair factors (DMC1, RAD51, RPA1A), DSB proteins (PRD1, PRD2, PRD3, SPO11-1, MTOPVIB) and meiotic chromosome axis proteins (ASY1, ASY3, SWI1 and REC8). Using serial dilutions, we observed that HCR1 shows strong interactions with REC8, SPO11-1, PRD1, RPA1A, MTOPVIB and PRD2 and weaker interactions with ASY1, RAD51, DMC1, ZYP1a and CDKA;1 (Fig. 6c,d and Extended Data Fig. 8a,b). Hence, although HCR1 represses the Class I crossover pathway, it may play a more widespread role regulating protein phosphorylation during Arabidopsis meiosis.

The human PP4 complex targets multiple proteins by recognizing a short motif (FxxP) via the PP4R3 Ena/Vasp Homology1 (EVH1) domain[61]. To explore whether a similar mechanism is relevant in Arabidopsis we performed yeast two-hybrid experiments using the Arabidopsis PP4R3A (At3g06670) EVH1 domain (residues 1-166) (Extended Data Figure 9). The PP4R3A-EVH1 domain interacts with 14 of 15 proteins observed as HCR1 interactors (Extended Data Figure 9). Additionally, PP4R3A showed two-hybrid interactions with PRD3 and SWI1 (Extended Data Figure 9). These data are consistent with HCR1/PPX1 and PP4R3A PP4 subunits interacting with a diverse set of proteins that regulate meiotic chromosomes and recombination, including Class I factors.

We sought to further test protein-protein interactions between HCR1 and Class I proteins *in planta*, using transient transfection and co-localization studies in Arabidopsis protoplasts (Fig. 6e). As reported[52], expression of a HCR1-CFP fusion protein showed nuclear localization (Fig. 6e). We co-expressed PPX1-CFP with PTD-YFP, HEI10-YFP, MSH5-YFP and MLH1-YFP fusion proteins and observed nuclear co-localization in all cases (Fig. 6e). We confirmed physical association of PPX1 using co-immunoprecipitation following transient expression in Arabidopsis protoplasts of PPX1-Myc, together with PTD-HA, HEI10-HA, MSH5-HA or MLH1-HA (Fig. 6f). In each case, these experiments confirmed that these proteins interact *in planta* (Fig. 6f).

As discussed, human protein phosphatase 4 (PP4) complexes bind the consensus motif FxxP, via the PP4R3A EVH1 domain[61] (Extended Data Fig. 9a,b and 10). Interestingly, 15 of 18 PPX1 interactors, and 12 of 16 PP4R3A-EVH1 interactors, identified using Y2H assays contain at least one FxxP motif (Extended Data Fig. 9, 10 and Supplementary Table 20). The PPX1 and PP4R3A interactors also possess multiple consensus sites used by CDK, DDK and ATM/ATR kinases (Extended Data Fig. 10c and Supplementary Table 20). We searched genome-wide for potential meiotic PP4 substrates according to the criteria of; (i) FxxP motifs (n=13,803), (ii) predicted nuclear location (n=10,595) and (iii) meiocyte-specific expression[34,61] (n=4,528). This search identified 1,367 candidate targets for the PP4 complex during meiosis

(Extended Data Fig. 10d). 1,315 of these proteins (96.2%) have at least one phosphorylation consensus site (Extended Data Fig. 10e). Furthermore, 15 of 18 PPX1 Y2H interactors, 12 of 16 PP4R3A-EVH1 Y2H interactors and 49 of 84 known meiotic proteins were included in this list of candidate PP4 substrates (Extended Data Fig. 10e and Supplementary Table 23). The proportion of candidate PP4 substrates (1,367) with at least one phosphorylation site is significantly higher than the random expectation (comparing to numbers of phosphorylation sites in 1,000 random sets of 1,367 proteins, *Z*-test $P=7.02\times10^{-31}$) (Extended Data Fig. 10f). The 1,367 predicted meiotic PP4 substrates are also significantly enriched in GO terms for DNA repair, DNA recombination, chromatin organization and meiosis I cell cycle (Extended Data Fig. 10g). Together this indicates the wide potential for PP4 regulation of meiosis and recombination in Arabidopsis.

Discussion

We identified the HCR1/PPX1 phosphatase as a repressor of crossover frequency in Arabidopsis. We provide genetic, cytological and protein-protein interaction data that a major target of HCR1/PPX1 is the Class I crossover pathway, with a minor role repressing Class II crossovers (Fig. 7). Our protein interaction data indicate that HEI10, PTD, MSH5 and MLH1 are likely direct targets for HCR1/PPX1 PP4 phosphatase activity within the Class I pathway. However, we also observed that HCR1/PPX1 and PP4R3A interact in a two-hybrid assay with components of the chromosome axis (ASY1, ASY3, REC8, SWI1), DSB proteins (SPO11-1, MTOPVIB, PRD1, PRD2) and recombinases (RPA1A, RAD51, DMC1), consistent with a broader regulatory role during meiosis.

In the absence of HCR1/PPX1, we propose that the action of pro-recombination kinases on the Class I pathway promotes stabilization of interhomolog strand invasion and crossover formation (Fig. 7). The crossover increases observed in *hcr1* and *meiMIGS-PPX1-PPX2* were most pronounced in the distal chromosome ends. Notably, distal crossover increases are characteristic of situations with elevated Class I activity in Arabidopsis, including male meiosis, *HEI10* and *CDKA;1*[36,62,63], although distal increases are also observed in mutants that increase Class II crossovers (e.g *recq4a recq4b*)[9,16,62]. The causes of distal biases in crossover formation in these backgrounds remain incompletely understood. Chromatin may be an important influence, as meiotic DSBs are elevated in gene-associated nucleosome-free regions, and there are positive associations with euchromatic chromatin marks, including H3K4me3 and H2A.Z[35,58,64,65]. In contrast, heterochromatic modifications including H3K9me2 and dense DNA methylation are associated with crossover suppression[33,66]. Additionally, Class I crossovers are subject to interference, which inhibits formation of adjacent crossovers in a distance-dependent manner[11]. A complete understanding of the crossover landscape in *hcr1* will require further investigation of how chromatin, chromosome structure and interference co-operate spatially and temporally during meiosis.

Within the Class I pathway, HEI10 belongs to a family of conserved ubiquitin or SUMO E3 ligases that promote interfering crossover formation in diverse eukaryotes[2,13]. In Arabidopsis, HEI10 is a dosage-sensitive promoter of Class I crossover repair[16,36]. HEI10 shows a dynamic localization pattern along plant meiotic chromosomes, initially showing numerous foci along the axis, which become restricted to a small number of foci that overlap MLH1 foci during late prophase I[12,67,68]. In budding yeast, the HEI10 ortholog Zip3 is phosphorylated in a DSB-dependent manner by Mec1 (ATR), which is antagonized by PPH3[22]. This is of particular interest as PPH3 is a HCR1/PPX1 ortholog, indicating that repression of the Class I pathway by PP4 phosphatases may be conserved between plants and fungi.

In mice, orthologs of HEI10 (e.g. RNF212) act to regulate association of the MutSy Msh4-Msh5 heterodimer with meiotic chromosomes[69,70]. Msh4-Msh5 heterodimers are capable of forming sliding clamps on DNA *in vitro* and associate with recombination foci along meiotic

chromosomes *in vivo*[71,72]. MutSy is proposed to bind nascent joint molecules and protect them from dissolution by anti-recombinases, including Sgs1-Top3-Rmi1 in budding yeast[71,73,74]. MutSy can also directly or indirectly recruit the MutLy (Mlh1-Mlh3) endonuclease heterodimer to promote crossover resolution[75–77]. Budding yeast Msh4 was recently identified as an intrinsically unstable protein that is degraded by the proteasome via an N-terminal degron[23]. Phosphorylation of the degron by the cell cycle kinase Cdc7-Dbf4 (DDK) inhibits Msh4 degradation and thereby promotes crossover repair[23]. As Arabidopsis HCR1/PPX1 physically interacts with MSH5 and MLH1 this may promote MutSy and MutLy dephosphorylation and thereby repress Class I crossover repair.

We observed physical interaction between HCR1/PPX1 and PTD, which is the partner protein of SHOC1, which together form a XPF-ERCC1-related complex[60,78–80]. Orthologs of the SHOC1-PTD complex include budding yeast Zip2-Spo16, which bind branched DNA molecules *in vitro*, lacks endonucleolytic activity and acts with Zip4 to promote crossover formation[80,81]. However, phosphorylation of Zip2-Spo16-Zip4 has been not reported in budding yeast or other organisms. Since Arabidopsis PTD interacts with HCR1 and PP4R3A-EVH1 and contains consensus phosphorylation sites, it is possible that plant SHOC1-PTD-ZIP4 complexes may be regulated by phosphorylation.

It is also possible that HCR1/PPX1 may regulate phosphorylation of the DSB machinery, or components of the meiotic chromosome axis, as observed in *Caenorhabditis elegans*[82]. Furthermore, orthologs of ASY1 (Hop1), REC8 (Rec8) and ZYP1 (Zip1) proteins in budding yeast are known to be regulated via phosphorylation[24,25]. Hence, it is possible that Arabidopsis ASY1, REC8 and ZYP1 may be dephosphorylated by PP4. However, we did not observe significant changes to RAD51 foci or ASY1 and ZYP1 immunostaining during meiosis in *hcr1* at the cytological level.

We consider three pro-recombination kinase pathways as candidates for HCR1/PPX1 PP4 antagonism (Fig. 7). First, cell division kinase (Cdk)-cyclin complexes are drivers of cell cycle progression, including during meiosis and are known to regulate recombination[18,63,83]. Second, Dbf4-dependent kinase (DDK) (Cdc7-Ddf4) plays a prominent role in the initiation of DNA replication, but also in regulation of recombination and kinetochore behaviour during meiosis[84–89]. Third, the ATM/ATR phosphatidylinositol 3-kinase-related kinases (PIKKs) are activated by DSBs and regulate meiotic DSB number and distribution in yeast and mammals[19–21]. Together these kinase pathways play complex and interacting roles in the promotion of crossovers during meiosis[90].

In Arabidopsis, CDKA;1 (the homolog of human Cdk1 and Cdk2) plays a role in promoting Class I crossovers[63,91]. Hence, HCR1/PPX1 may remove phosphorylation from CDKA;1 targets within the Class I pathway and thereby limit crossovers (Fig. 7). Interestingly, mutation of CDK consensus motifs (S/T-P) in budding yeast Zip3 had no effect on phosphorylation, whereas mutation of Tel1/Mec1 sites (S/T-Q) did[22]. As noted earlier, Zip3 phosphorylation has been shown to be regulated by PP4[22], meaning that HCR1 may regulate HEI10 phosphorylation in an analogous manner in Arabidopsis (Fig. 7). Indeed, it has been shown that many Mec1 phospho-targets, including Zip1, are also PP4 substrates in budding yeast[49]. In Arabidopsis ATM and ATR are redundantly required for DSB repair[92]. The *atm* single mutant is partially sterile with increased meiotic DSBs, chromosomal fragmentation and moderately increased Class I crossovers[93,94]. In budding yeast, DDK is responsible for Msh4 degron phosphorylation and stabilization[23]. Hence, it is possible that HCR1 could remove phosphorylation from MutSy and thereby promote its destabilization and repress crossovers (Fig. 7). However, the meiotic function of DDK kinases in plants is currently unknown.

Studies in diverse systems and contexts have identified PP4 phosphatase complexes as key regulators of DNA repair and recombination. For example, the DNA damage response

involves kinase regulation, which is balanced with antagonising phosphatases[41]. Defined roles for PP4 complexes include; (i) dephosphorylation of gamma-H2AX during recovery from DNA damage checkpoints in Drosophila, budding yeast and human[42–45], (ii) prevention of Rad53 hyperphosphorylation during DSB repair and promoting DNA end resection in budding yeast[95], (iii) dephosphorylating RPA2 to promote DNA repair via homologous recombination[27], (iv) promoting NHEJ-mediated DSB repair, which occurs partially via KRAB-associated protein1 (KAP1)[48], (v) regulation of Mec1 during DSB repair and at sites of replication fork collapse[26], and (vi) regulating Zip1 phosphorylation during meiosis to control homology-independent centromere pairing[49]. Our work identifies PPX1-PP4 phosphatase complexes as repressing the Class I crossover pathway during Arabidopsis meiosis. We propose that PP4 complexes may generally act in opposition to pro-recombination kinases to regulate meiotic crossovers in eukaryotes.

References

1. Villeneuve, A. M. & Hillers, K. J. Whence meiosis? *Cell* **106**, 647–50 (2001).
2. Mercier, R., Mézard, C., Jenczewski, E., Macaisne, N. & Grelon, M. The molecular biology of meiosis in plants. *Annu. Rev. Plant Biol.* **66**, 297–327 (2015).
3. Grelon, M., Vezon, D., Gendrot, G. & Pelletier, G. AtSPO11-1 is necessary for efficient meiotic recombination in plants. *EMBO J.* **20**, 589–600 (2001).
4. Robert, T. *et al.* The TopoVIB-Like protein family is required for meiotic DNA double-strand break formation. *Science (80-.).* **351**, 943–949 (2016).
5. Hartung, F. *et al.* The catalytically active tyrosine residues of both SPO11-1 and SPO11-2 are required for meiotic double-strand break induction in Arabidopsis. *Plant Cell* **19**, 3090–9 (2007).
6. Hunter, N. Meiotic Recombination: The Essence of Heredity. *Cold Spring Harb. Perspect. Biol.* **7**, a016618 (2015).
7. Ferdous, M. *et al.* Inter-homolog crossing-over and synapsis in Arabidopsis meiosis are dependent on the chromosome axis protein AtASY3. *PLoS Genet.* **8**, e1002507 (2012).
8. Rowan, B. A. *et al.* An Ultra High-Density Arabidopsis thaliana Crossover Map That Refines the Influences of Structural Variation and Epigenetic Features. *Genetics* **213**, 771–787 (2019).
9. Girard, C. *et al.* AAA-ATPase FIDGETIN-LIKE 1 and Helicase FANCM Antagonize Meiotic Crossovers by Distinct Mechanisms. *PLoS Genet.* **11**, e1005369 (2015).
10. Cifuentes, M., Rivard, M., Pereira, L., Chelysheva, L. & Mercier, R. Haploid Meiosis in Arabidopsis: Double-Strand Breaks Are Formed and Repaired but Without Synapsis and Crossovers. *PLoS One* **8**, e72431 (2013).
11. Berchowitz, L. E. & Copenhaver, G. P. Genetic interference: don't stand so close to me. *Curr. Genomics* **11**, 91–102 (2010).
12. Li, Y. *et al.* HEIP1 regulates crossover formation during meiosis in rice. *Proc. Natl. Acad. Sci.* **115**, 10810–10815 (2018).
13. Pyatnitskaya, A., Borde, V. & De Muyt, A. Crossing and zipping: molecular duties of the ZMM proteins in meiosis. *Chromosoma* **128**, 181–198 (2019).
14. Mercier, R. *et al.* Two meiotic crossover classes cohabit in Arabidopsis: one is dependent on MER3,whereas the other one is not. *Curr. Biol.* **15**, 692–701 (2005).
15. Séguéla-Arnaud, M. *et al.* Multiple mechanisms limit meiotic crossovers: TOP3α and two BLM homologs antagonize crossovers in parallel to FANCM. *Proc. Natl. Acad. Sci. U. S. A.* **112**, 4713–8 (2015).
16. Serra, H. *et al.* Massive crossover elevation via combination of HEI10 and recq4a recq4b during Arabidopsis meiosis. *Proc. Natl. Acad. Sci. U. S. A.* **115**, 2437–2442 (2018).
17. Marston, A. L. & Amon, A. Meiosis: Cell-cycle controls shuffle and deal. *Nature*

Reviews Molecular Cell Biology vol. 5 983–997 (2004).
18. Yang, C. *et al.* The Arabidopsis Cdk1/Cdk2 homolog CDKA ;1 controls chromosome axis assembly during plant meiosis . *EMBO J.* **39**, 1–19 (2020).
19. Lange, J. *et al.* The Landscape of Mouse Meiotic Double-Strand Break Formation, Processing, and Repair. *Cell* **167**, 695-708.e16 (2016).
20. Garcia, V., Gray, S., Allison, R. M., Cooper, T. J. & Neale, M. J. Tel1(ATM)-mediated interference suppresses clustered meiotic double-strand-break formation. *Nature* **520**, 114–118 (2015).
21. Lange, J. *et al.* ATM controls meiotic double-strand-break formation. *Nature* **479**, 237–40 (2011).
22. Serrentino, M.-E., Chaplais, E., Sommermeyer, V. & Borde, V. Differential association of the conserved SUMO ligase Zip3 with meiotic double-strand break sites reveals regional variations in the outcome of meiotic recombination. *PLoS Genet.* **9**, e1003416 (2013).
23. He, W. *et al.* Regulated Proteolysis of MutSγ Controls Meiotic Crossing Over. *Mol. Cell* **78**, 168-183.e5 (2020).
24. Carballo, J. A., Johnson, A. L., Sedgwick, S. G. & Cha, R. S. Phosphorylation of the axial element protein Hop1 by Mec1/Tel1 ensures meiotic interhomolog recombination. *Cell* **132**, 758–70 (2008).
25. Brar, G. A. *et al.* Rec8 phosphorylation and recombination promote the step-wise loss of cohesins in meiosis. *Nature* **441**, 532–536 (2006).
26. Hustedt, N. *et al.* Yeast PP4 interacts with ATR homolog Ddc2-Mec1 and regulates checkpoint signaling. *Mol. Cell* **57**, 273–289 (2015).
27. Lee, D. H. *et al.* A PP4 phosphatase complex dephosphorylates RPA2 to facilitate DNA repair via homologous recombination. *Nat. Struct. Mol. Biol.* **17**, 365–372 (2010).
28. Wang, S. *et al.* The PROTEIN PHOSPHATASE4 Complex Promotes Transcription and Processing of Primary microRNAs in Arabidopsis. *Plant Cell* **31**, 486–501 (2019).
29. Wu, G., Rossidivito, G., Hu, T., Berlyand, Y. & Poethig, R. S. Traffic lines: new tools for genetic analysis in Arabidopsis thaliana. *Genetics* **200**, 35–45 (2015).
30. Melamed-Bessudo, C., Yehuda, E., Stuitje, A. R. & Levy, A. A. A new seed-based assay for meiotic recombination in Arabidopsis thaliana. *Plant J.* **43**, 458–66 (2005).
31. Berchowitz, L. E. & Copenhaver, G. P. Fluorescent Arabidopsis tetrads: a visual assay for quickly developing large crossover and crossover interference data sets. *Nat. Protoc.* **3**, 41–50 (2008).
32. Ziolkowski, P. A. *et al.* Juxtaposition of heterozygous and homozygous regions causes reciprocal crossover remodelling via interference during Arabidopsis meiosis. *Elife* **4**, e03708 (2015).
33. Yelina, N. E. *et al.* DNA methylation epigenetically silences crossover hot spots and controls chromosomal domains of meiotic recombination in Arabidopsis. *Genes Dev.* **29**, 2183–202 (2015).
34. Lawrence, E. J. *et al.* Natural Variation in TBP-ASSOCIATED FACTOR 4b Controls Meiotic Crossover and Germline Transcription in Arabidopsis. *Curr. Biol.* **29**, 2676–2686 (2019).
35. Choi, K. *et al.* Arabidopsis meiotic crossover hot spots overlap with H2A.Z nucleosomes at gene promoters. *Nat. Genet.* **45**, 1327–36 (2013).
36. Ziolkowski, P. A. *et al.* Natural variation and dosage of the HEI10 meiotic E3 ligase control Arabidopsis crossover recombination. *Genes Dev.* **31**, 306–317 (2017).
37. Crismani, W. *et al.* FANCM limits meiotic crossovers. *Science* **336**, 1588–90 (2012).
38. Allen, R., Nakasugi, K., Doran, R. L., Millar, A. A. & Waterhouse, P. M. Facile mutant identification via a single parental backcross method and application of whole genome sequencing based mapping pipelines. *Front. Plant Sci.* **4**, 1–8 (2013).
39. Shi, Y. Serine/Threonine Phosphatases: Mechanism through Structure. *Cell* vol. 139 468–484 (2009).
40. Gingras, A. C. *et al.* A novel, evolutionarily conserved protein phosphatase complex

involved in cisplatin sensitivity. *Mol. Cell. Proteomics* **4**, 1725–1740 (2005).
41. Ramos, F., Villoria, M. T., Alonso-Rodríguez, E. & Clemente-Blanco, A. Role of protein phosphatases PP1, PP2A, PP4 and Cdc14 in the DNA damage response. *Cell Stress* (2019) doi:10.15698/cst2019.03.178.
42. Nakada, S., Chen, G. I., Gingras, A. C. & Durocher, D. PP4 is a γH2AX phosphatase required for recovery from the DNA damage checkpoint. *EMBO Rep.* (2008) doi:10.1038/embor.2008.162.
43. Chowdhury, D. *et al.* A PP4-Phosphatase Complex Dephosphorylates γ-H2AX Generated during DNA Replication. *Mol. Cell* (2008) doi:10.1016/j.molcel.2008.05.016.
44. Merigliano, C. *et al.* A role for the twins protein phosphatase (PP2A-B55) in the maintenance of Drosophila genome integrity. *Genetics* (2017) doi:10.1534/genetics.116.192781.
45. Keogh, M. C. *et al.* A phosphatase complex that dephosphorylates γH2AX regulates DNA damage checkpoint recovery. *Nature* (2006) doi:10.1038/nature04384.
46. O'Neill, B. M. *et al.* Pph3-Psy2 is a phosphatase complex required for Rad53 dephosphorylation and replication fork restart during recovery from DNA damage. *Proc. Natl. Acad. Sci. U. S. A.* (2007) doi:10.1073/pnas.0703252104.
47. Lee, D. H. *et al.* A PP4 phosphatase complex dephosphorylates RPA2 to facilitate DNA repair via homologous recombination. *Nat. Struct. Mol. Biol.* (2010) doi:10.1038/nsmb.1769.
48. Liu, J. *et al.* Protein phosphatase PP4 is involved in NHEJ-mediated repair of DNA double-strand breaks. *Cell Cycle* (2012) doi:10.4161/cc.20957.
49. Falk, J. E. J., Chan, A. C. A. ho A., Hoffmann, E. & Hochwagen, A. A Mec1- and PP4-Dependent checkpoint couples centromere pairing to meiotic recombination. *Dev. Cell* **19**, 599–611 (2010).
50. Pérez-Callejón, E. *et al.* Identification and molecular cloning of two homologues of protein phosphatase X from Arabidopsis thaliana. *Plant Mol. Biol.* **23**, 1177–1185 (1993).
51. Moorhead, G. B. G., De Wever, V., Templeton, G. & Kerk, D. Evolution of protein phosphatases in plants and animals. *Biochem. J.* **417**, 401–409 (2009).
52. Su, C. *et al.* The Protein Phosphatase 4 and SMEK1 Complex Dephosphorylates HYL1 to Promote miRNA Biogenesis by Antagonizing the MAPK Cascade in Arabidopsis. *Dev. Cell* **41**, 527-539.e5 (2017).
53. de Felippes, F. F., Wang, J. & Weigel, D. MIGS: miRNA-induced gene silencing. *Plant J.* **70**, 541–547 (2012).
54. Klimyuk, V. I. & Jones, J. D. AtDMC1, the Arabidopsis homologue of the yeast DMC1 gene: characterization, transposon-induced allelic variation and meiosis-associated expression. *Plant J.* **11**, 1–14 (1997).
55. Lim, E. C. *et al.* DeepTetrad: high-throughput image analysis of meiotic tetrads by deep learning in Arabidopsis thaliana. *Plant J.* **101**, 473–483 (2020).
56. Rowan, B. A., Patel, V., Weigel, D. & Schneeberger, K. Rapid and Inexpensive Whole-Genome Genotyping-by-Sequencing for Crossover Localization and Fine-Scale Genetic Mapping. *G3 (Bethesda).* **5**, 385–98 (2015).
57. Choi, K. *et al.* Recombination Rate Heterogeneity within Arabidopsis Disease Resistance Genes. *PLoS Genet.* **12**, e1006179 (2016).
58. Choi, K. *et al.* Nucleosomes and DNA methylation shape meiotic DSB frequency in Arabidopsis thaliana transposons and gene regulatory regions. *Genome Res.* **28**, 532–546 (2018).
59. Zhang, J. *et al.* A multiprotein complex regulates interference-sensitive crossover formation in rice. *Plant Physiol.* **181**, 221–235 (2019).
60. Macaisne, N., Vignard, J. & Mercier, R. SHOC1 and PTD form an XPF-ERCC1-like complex that is required for formation of class I crossovers. *J. Cell Sci.* **124**, 2687–91 (2011).

61. Ueki, Y. *et al.* A Consensus Binding Motif for the PP4 Protein Phosphatase. *Mol. Cell* (2019) doi:10.1016/j.molcel.2019.08.029.
62. Fernandes, J. B., Seguela-Arnaud, M., Larcheveque, C., Lloyd, A. H. & Mercier, R. Unleashing meiotic crossovers in hybrid plants. *Proc. Natl. Acad. Sci. U. S. A.* **115**, 2431–2436 (2017).
63. Wijnker, E. *et al.* The Cdk1/Cdk2 homolog CDKA;1 controls the recombination landscape in Arabidopsis. *Proc. Natl. Acad. Sci. U. S. A.* 201820753 (2019) doi:10.1073/pnas.1820753116.
64. He, Y. *et al.* Genomic features shaping the landscape of meiotic double-strand-break hotspots in maize. *Proc. Natl. Acad. Sci. U. S. A.* **114**, 12231–12236 (2017).
65. Liu, S. *et al.* Mu Transposon Insertion Sites and Meiotic Recombination Events Co-Localize with Epigenetic Marks for Open Chromatin across the Maize Genome. *PLoS Genet.* **5**, e1000733 (2009).
66. Underwood, C. J. *et al.* Epigenetic activation of meiotic recombination near Arabidopsis thaliana centromeres via loss of H3K9me2 and non-CG DNA methylation. *Genome Res.* **28**, 519–531 (2018).
67. Chelysheva, L. *et al.* The Arabidopsis HEI10 is a new ZMM protein related to Zip3. *PLoS Genet.* **8**, e1002799 (2012).
68. Wang, K. *et al.* The role of rice HEI10 in the formation of meiotic crossovers. *PLoS Genet.* **8**, e1002809 (2012).
69. Reynolds, A. *et al.* RNF212 is a dosage-sensitive regulator of crossing-over during mammalian meiosis. *Nat. Genet.* **45**, 269–78 (2013).
70. Qiao, H. *et al.* Antagonistic roles of ubiquitin ligase HEI10 and SUMO ligase RNF212 regulate meiotic recombination. *Nat. Genet.* **46**, 194–9 (2014).
71. Woglar, A. & Villeneuve, A. M. Dynamic Architecture of DNA Repair Complexes and the Synaptonemal Complex at Sites of Meiotic Recombination. *Cell* **173**, 1678-1691.e16 (2018).
72. Snowden, T., Acharya, S., Butz, C., Berardini, M. & Fishel, R. hMSH4-hMSH5 recognizes Holliday Junctions and forms a meiosis-specific sliding clamp that embraces homologous chromosomes. *Mol. Cell* **15**, 437–51 (2004).
73. Jessop, L., Rockmill, B., Roeder, G. S. & Lichten, M. Meiotic chromosome synapsis-promoting proteins antagonize the anti-crossover activity of sgs1. *PLoS Genet.* **2**, e155 (2006).
74. Oh, S. D., Lao, J. P., Taylor, A. F., Smith, G. R. & Hunter, N. RecQ Helicase, Sgs1, and XPF Family Endonuclease, Mus81-Mms4, Resolve Aberrant Joint Molecules during Meiotic Recombination. *Mol. Cell* **31**, 324–336 (2008).
75. Manhart, C. M. *et al.* The mismatch repair and meiotic recombination endonuclease Mlh1-Mlh3 is activated by polymer formation and can cleave DNA substrates in trans. *PLOS Biol.* **15**, e2001164 (2017).
76. Zakharyevich, K., Tang, S., Ma, Y. & Hunter, N. Delineation of joint molecule resolution pathways in meiosis identifies a crossover-specific resolvase. *Cell* **149**, 334–47 (2012).
77. Ranjha, L., Anand, R. & Cejka, P. The Saccharomyces cerevisiae Mlh1-Mlh3 heterodimer is an endonuclease that preferentially binds to holliday junctions. *J. Biol. Chem.* **289**, 5674–5686 (2014).
78. Wijeratne, A. J., Chen, C., Zhang, W., Timofejeva, L. & Ma, H. The Arabidopsis thaliana PARTING DANCERS gene encoding a novel protein is required for normal meiotic homologous recombination. *Mol. Biol. Cell* **17**, 1331–43 (2006).
79. Lu, P., Wijeratne, A. J., Wang, Z., Copenhaver, G. P. & Ma, H. Arabidopsis PTD is required for type I crossover formation and affects recombination frequency in two different chromosomal regions. *J. Genet. Genomics* **41**, 165–75 (2014).
80. De Muyt, A. *et al.* A meiotic XPF–ERCC1-like complex recognizes joint molecule recombination intermediates to promote crossover formation. *Genes Dev.* **32**, 283–296 (2018).

81. Arora, K. & Corbett, K. D. The conserved XPF:ERCC1-like Zip2:Spo16 complex controls meiotic crossover formation through structure-specific DNA binding. *Nucleic Acids Res.* **47**, 2365–2376 (2019).
82. Sato-Carlton, A. *et al.* Protein Phosphatase 4 Promotes Chromosome Pairing and Synapsis, and Contributes to Maintaining Crossover Competence with Increasing Age. *PLoS Genet.* **10**, e1004638 (2014).
83. Henderson, K. A., Kee, K., Maleki, S., Santini, P. A. & Keeney, S. Cyclin-dependent kinase directly regulates initiation of meiotic recombination. *Cell* **125**, 1321–32 (2006).
84. Lam, I. & Keeney, S. Mechanism and Regulation of Meiotic Recombination Initiation. *Cold Spring Harb. Perspect. Biol.* **7**, a016634 (2014).
85. Valentin, G., Schwob, E. & Della Seta, F. Dual role of the Cdc7-regulatory protein Dbf4 during yeast meiosis. *J. Biol. Chem.* **281**, 2828–2834 (2006).
86. Sasanuma, H. *et al.* Cdc7-dependent phosphorylation of Mer2 facilitates initiation of yeast meiotic recombination. *Genes Dev.* **22**, 398–410 (2008).
87. Wan, L. *et al.* Cdc28-Clb5 (CDK-S) and Cdc7-Dbf4 (DDK) collaborate to initiate meiotic recombination in yeast. *Genes Dev.* **22**, 386–397 (2008).
88. Matos, J. *et al.* Dbf4-Dependent Cdc7 Kinase Links DNA Replication to the Segregation of Homologous Chromosomes in Meiosis I. *Cell* **135**, 662–678 (2008).
89. Chen, X. *et al.* Phosphorylation of the Synaptonemal Complex Protein Zip1 Regulates the Crossover/Noncrossover Decision during Yeast Meiosis. *PLOS Biol.* **13**, e1002329 (2015).
90. Keeney, S., Lange, J. & Mohibullah, N. Self-organization of meiotic recombination initiation: general principles and molecular pathways. *Annu. Rev. Genet.* **48**, 187–214 (2014).
91. Nowack, M. K. *et al.* Genetic Framework of Cyclin-Dependent Kinase Function in Arabidopsis. *Dev. Cell* **22**, 1030–1040 (2012).
92. Culligan, K. M. & Britt, A. B. Both ATM and ATR promote the efficient and accurate processing of programmed meiotic double-strand breaks. *Plant J.* **55**, 629–638 (2008).
93. Garcia, V. *et al.* AtATM is essential for meiosis and the somatic response to DNA damage in plants. *Plant Cell* **15**, 119–32 (2003).
94. Yao, Y. *et al.* ATM Promotes RAD51-Mediated Meiotic DSB Repair by Inter-Sister-Chromatid Recombination in Arabidopsis. *Front. Plant Sci.* **11**, (2020).
95. Villoria, M. T. *et al.* PP4 phosphatase cooperates in recombinational DNA repair by enhancing double-strand break end resection. *Nucleic Acids Res.* (2019) doi:10.1093/nar/gkz794.
96. Chelysheva, L. *et al.* Zip4/Spo22 is required for class I CO formation but not for synapsis completion in Arabidopsis thaliana. *PLoS Genet.* **3**, e83 (2007).
97. van Tol, N., Rolloos, M., van Loon, P. & van der Zaal, B. J. MeioSeed: a CellProfiler-based program to count fluorescent seeds for crossover frequency analysis in Arabidopsis thaliana. *Plant Methods* **14**, 32 (2018).
98. Carpenter, A. E. *et al.* CellProfiler: image analysis software for identifying and quantifying cell phenotypes. *Genome Biol.* **7**, R100 (2006).
99. Zhang, X., Henriques, R., Lin, S. S., Niu, Q. W. & Chua, N. H. Agrobacterium-mediated transformation of Arabidopsis thaliana using the floral dip method. *Nat. Protoc.* **1**, 641–646 (2006).
100. Chelysheva, L. *et al.* An easy protocol for studying chromatin and recombination protein dynamics during Arabidopsis thaliana meiosis: immunodetection of cohesins, histones and MLH1. *Cytogenet. Genome Res.* **129**, 143–53 (2010).
101. Lambing, C., Kuo, P. C., Tock, A. J., Topp, S. D. & Henderson, I. R. ASY1 acts as a dosage-dependent antagonist of telomere-led recombination and mediates crossover interference in Arabidopsis. *Proc. Natl. Acad. Sci. U. S. A.* **24**, 13647–13658 (2020).
102. Sanchez-Moran, E., Santos, J.-L., Jones, G. H. & Franklin, F. C. H. ASY1 mediates AtDMC1-dependent interhomolog recombination during meiosis in Arabidopsis.

Genes Dev. **21**, 2220–33 (2007).
103. Higgins, J. D., Sanchez-Moran, E., Armstrong, S. J., Jones, G. H. & Franklin, F. C. H. The Arabidopsis synaptonemal complex protein ZYP1 is required for chromosome synapsis and normal fidelity of crossing over. *Genes Dev.* **19**, 2488–2500 (2005).
104. Hwang, I. & Sheen, J. Two-component circuitry in Arabidopsis cytokinin signal transduction. *Nature* **413**, 383–389 (2001).
105. Xue, Y. *et al.* GPS 2.1: Enhanced prediction of kinase-specific phosphorylation sites with an algorithm of motif length selection. *Protein Eng. Des. Sel.* **24**, 255–260 (2011).

Acknowledgments

We thank Gregory Copenhaver (University of North Carolina), Avraham Levy (The Weizmann Institute), and Scott Poethig (University of Pennsylvania) for FTLs/CTLs, Raphael Mercier (Max Planck Institute, Cologne) for *fancm-1*, Liliana Ziolkowska and Charles Underwood (Max Planck Institute, Cologne) for helping grow the EMS population, Mathilde Grelon (INRA, Versailles) for MLH1 antibodies, Chris Franklin (University of Birmingham) for ASY1, ZYP1 and RAD51 antibodies and the Gurdon Institute for access to microscopes. This work was funded by the Suh Kyungbae Foundation (JaK, JuK, JP, EK, HK, DB, YMP, KC), Next-Generation BioGreen 21 Program PJ01337001 (JaK, JuK, JP, EK, HK, DB, YMP, KC) and PJ01342301 (HSC, SL, IH), Rural Development Administration, Basic Science Research Program through the National Research Foundation of Korea (NRF) funded by the Ministry of Education NRF-2020R1A2C2007763 (HK, DB, KC), Marie-Curie International Training Network 'COMREC' (DN), BBSRC grant EpiSpiX BB/N007557/1 (XZ, IH), BBSRC ERA-CAPs grant BB/M004937/1 (CL, IH) and ERC Consolidator Award ERC-2015-CoG-681987 'SynthHotSpot' (CL, AT, IH).

Author Contributions Statement

Design and conception of experiments: DN, JaK, CL, JuK, JP, EK, PK, KC, IH.
Acquisition and analysis of data: DN, JaK, CL, JuK, JP, HSC, HK, DB, YMP, PK, SL, AT, XZ, IH, KC.
Wrote the manuscript: DN, JaK, CL, JuK, KC, IH.

Competing Interests Statement

The authors declare no competing financial or non-financial interests in relation to this work.

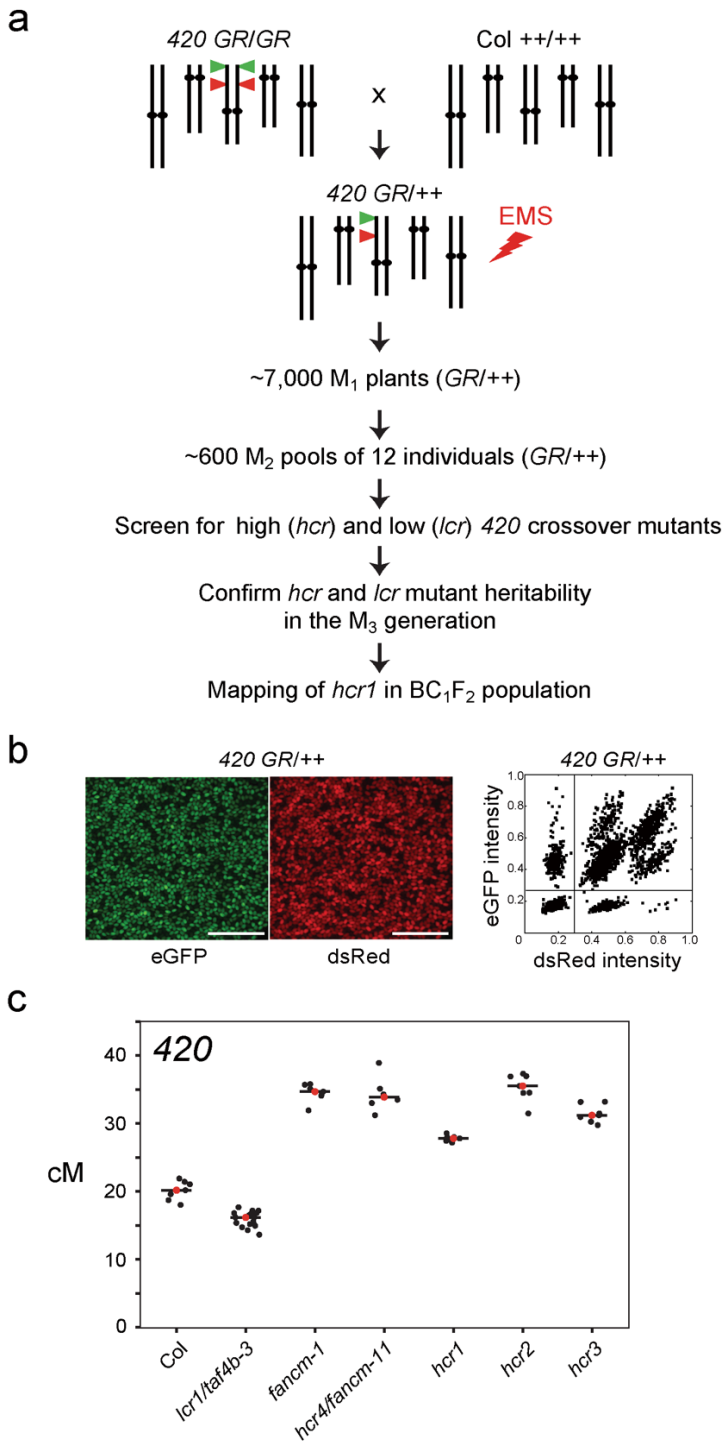

Figure 1. A forward genetic screen for mutants with changed *420* crossover frequency. **a,** Schematic diagram of a forward genetic screen for identifying high (*hcr*) or low (*lcr*) crossover mutants, using the *420* FTL crossover reporter interval (green and red triangles on chromosome 3). *420/++* seed were EMS treated and the subsequent steps followed to identify the *hcr1* mutant. **b,** Representative fluorescent micrographs of *420/++* seeds. Scale bars=5 mm. A representative plot of red (dsRed) and green (eGFP) fluorescence values from *420/++* seed is shown alongside. Vertical and horizontal lines indicate thresholds for colour:non-colour classifications used for crossover frequency estimation. **c,** *420* crossover frequency (cM) in wild type, *fancm*, *hcr* and *lcr* mutants. Mean values are indicated by red dots and the black horizontal bar.

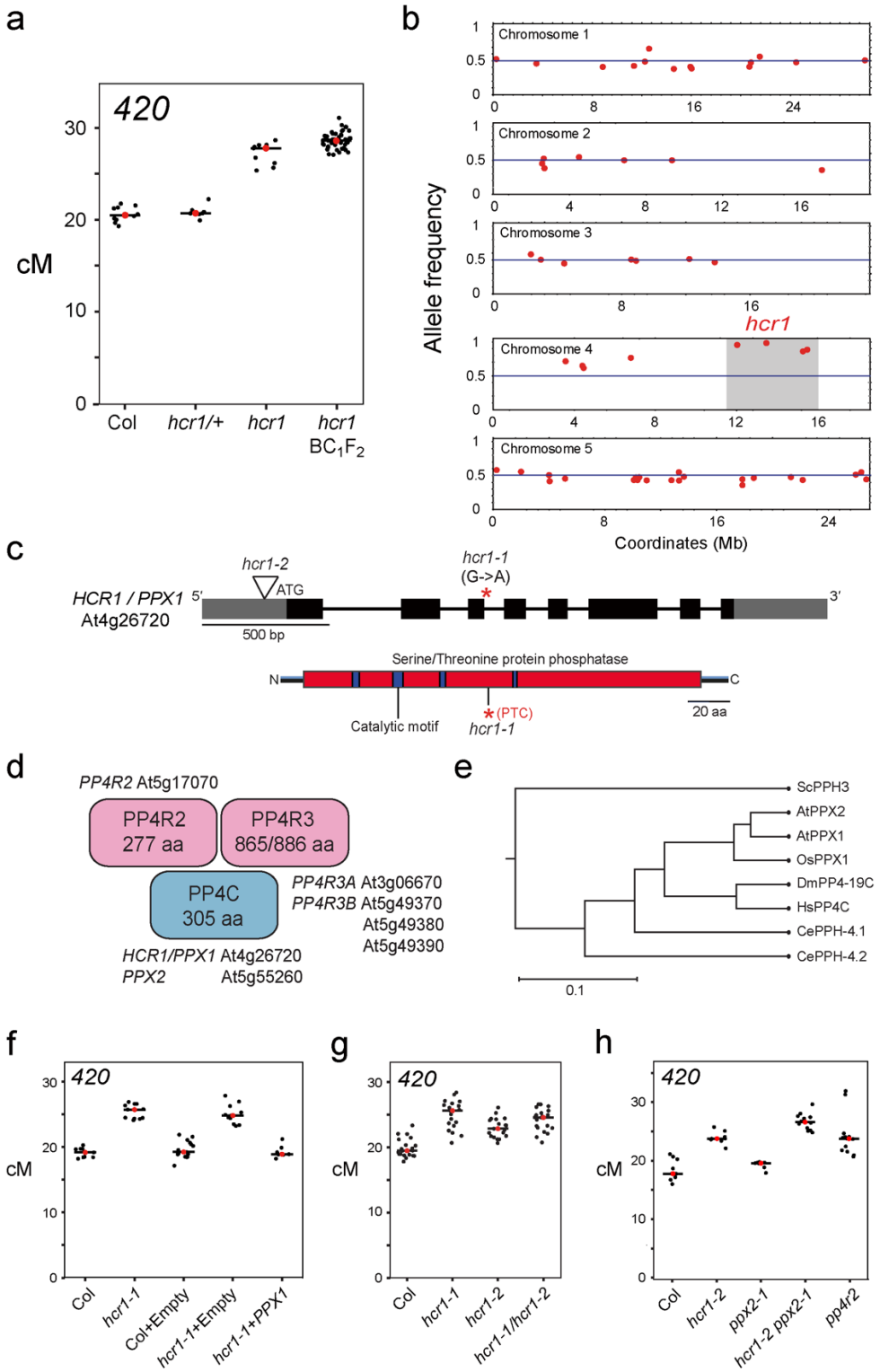

Figure 2. ***HIGH CROSSOVER RATE1*** **encodes PROTEIN PHOSPHATASE X1. a,** *420* crossover frequency (cM) in wild type, *hcr1-1, hcr1-1/+* and high recombination *hcr1-1* BC_1F_2 individuals used for DNA extraction and mapping-by-sequencing. Mean cM values are indicated by red dots and horizontal lines. **b,** Allele frequency of EMS mutations (red) identified by SHOREmap in high recombination *hcr1-1* BC_1F_2 individuals. The blue horizontal line indicates 0.5 allele frequency. The *hcr1-1* candidate region and mutations are highlighted on chromosome 4 with grey shading. **c,** *HCR1/PPX1* gene with exons shown as boxes (black=CDS, grey=UTR) and the position of the *hcr1-1* substitution. The *hcr1-2* T-DNA

insertion (triangle) is located in the gene 5´-UTR (triangle). A diagram of the HCR1/PPX1 protein is shown indicating the serine/threonine protein phosphatase domain (red), catalytic motifs (blue) and the position of the premature stop codon (*,PTC) caused by *hcr1-1*. **d,** A representation of the PP4 phosphatase complex with subunits (PP4C, PP4R2, PP4R3) shown and cognate Arabidopsis homologous genes. **e,** PPX/PP4C neighbor joining phylogenetic tree based on an alignment of amino acid sequences. The scale bar represents the number of changes per amino acid position. **f,** As for a, but showing *420* crossover frequency in *hcr1-1* after transformation with *PPX1* or empty vector constructs. **g,** As for a, but showing *420* crossover frequency in *hcr1-1, hcr1-2* and *hcr1-1/hcr1-2* F_1 hybrids. **h,** *420* crossover frequency in the *hcr1-2, ppx2* and *pp4r2* mutants.

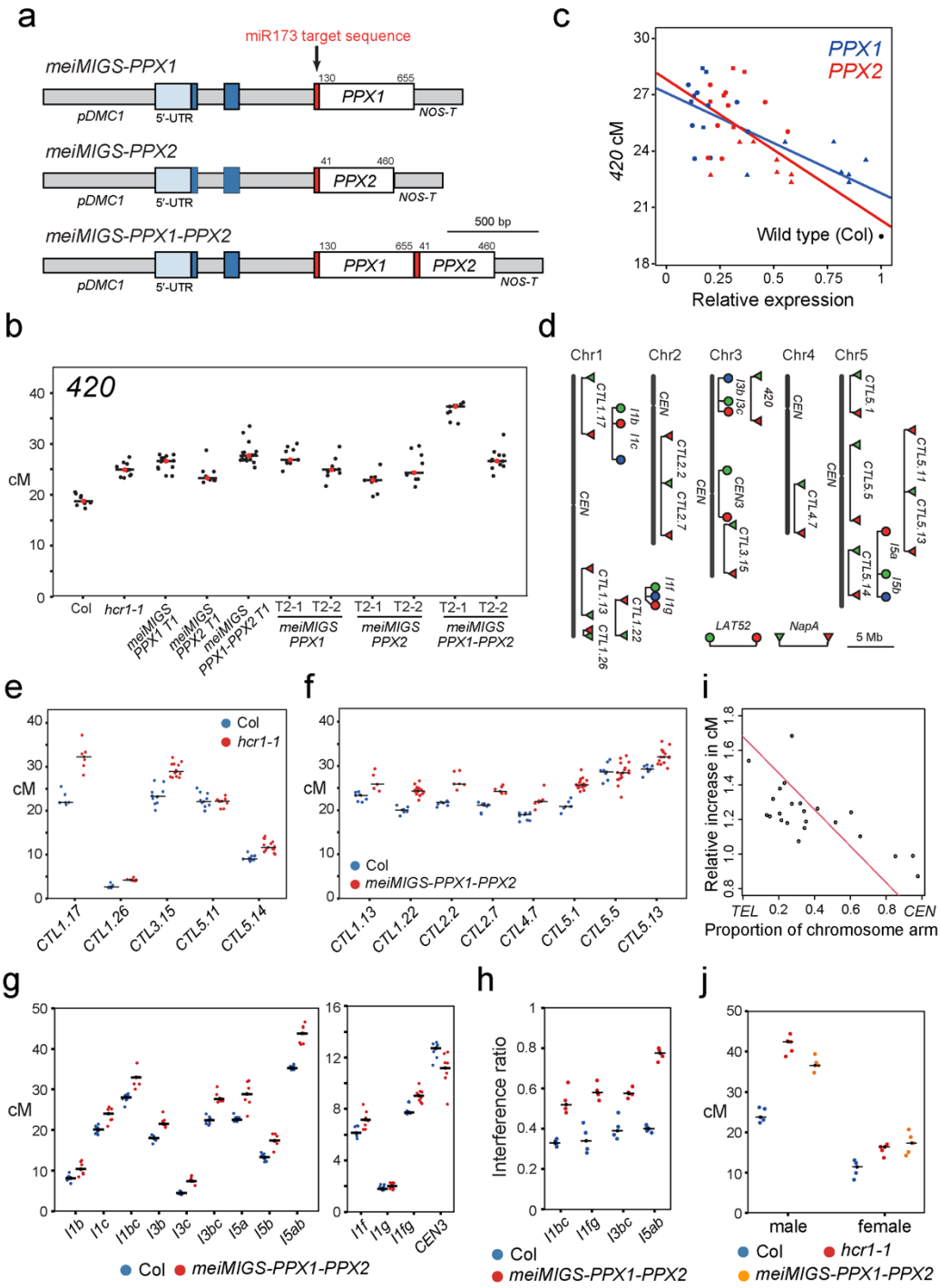

Figure 3. Euchromatic crossover frequency increases and crossover interference decreases in *hcr1* and *meiMIGS-PPX1-PPX2*. a, Graphical representation of the *meiMIGS-PPX1*, *meiMIGS-PPX2* and *meiMIGS-PPX1-PPX2* constructs. **b,** *420* crossover frequency (cM) in wild type, *meiMIGS-PPX1*, *meiMIGS-PPX2* and *meiMIGS-PPX1-PPX2* T_1 and T_2 transgenic lines. **c,** Correlation between *420* cM and *PPX1/HCR1* and *PPX2* transcript levels in floral buds of wild type and *meiMIGS-PPX1*, *meiMIGS-PPX2* and *meiMIGS-PPX1-PPX2* T_2 transgenic lines. The y axis represents *420* cM and x axis indicates fold-enrichment of *PPX1* (blue) and *PPX2* (red) transcript levels compared to *PPX1* and *PPX2* in wild type in RT-qPCR analysis. *DMC1* was used as a meiotic gene for normalization. Mean values of triple replicate RT-qPCRs were used. Wild type (Col), *meiMIGS-PPX1*, *meiMIGS-PPX2* and *meiMIGS-PPX1-PPX2* plants are shown as a black circle, red or blue-circles, -triangles and -squares,

respectively. **d,** FTL T-DNA intervals throughout the Arabidopsis genome used to measure crossover frequency. Circles indicate *LAT52*-driven, and triangles indicate *NapA*-driven FTL transgenes. **e,** As for c, but showing FTL crossover frequency in wild type (blue) and *hcr1-1* (red). Mean values are indicated by horizontal black lines. **f,** As for c, but showing FTL crossover frequency in wild type (blue) and *meiMIGS-PPX1-PPX2* (red). **g,** As for c, but showing pollen-based FTL crossover frequency in wild type (blue) and *meiMIGS-PPX1-PPX2* (red). **h,** Crossover interference ratio measured using FTL pollen tetrads in wild type (blue) compared with *meiMIGS-PPX1-PPX2* (red). **i,** Correlation between FTL cM change in *hcr1-1* or *meiMIGS-PPX1-PPX2* and the midpoint of the FTL interval analysed relative to the telomere (*TEL*) and centromere (*CEN*). **j,** *420* crossover frequency (cM) in male and female meiosis of wild type (blue), *hcr1-1* (red) and *meiMIGS-PPX1-PPX2* (orange).

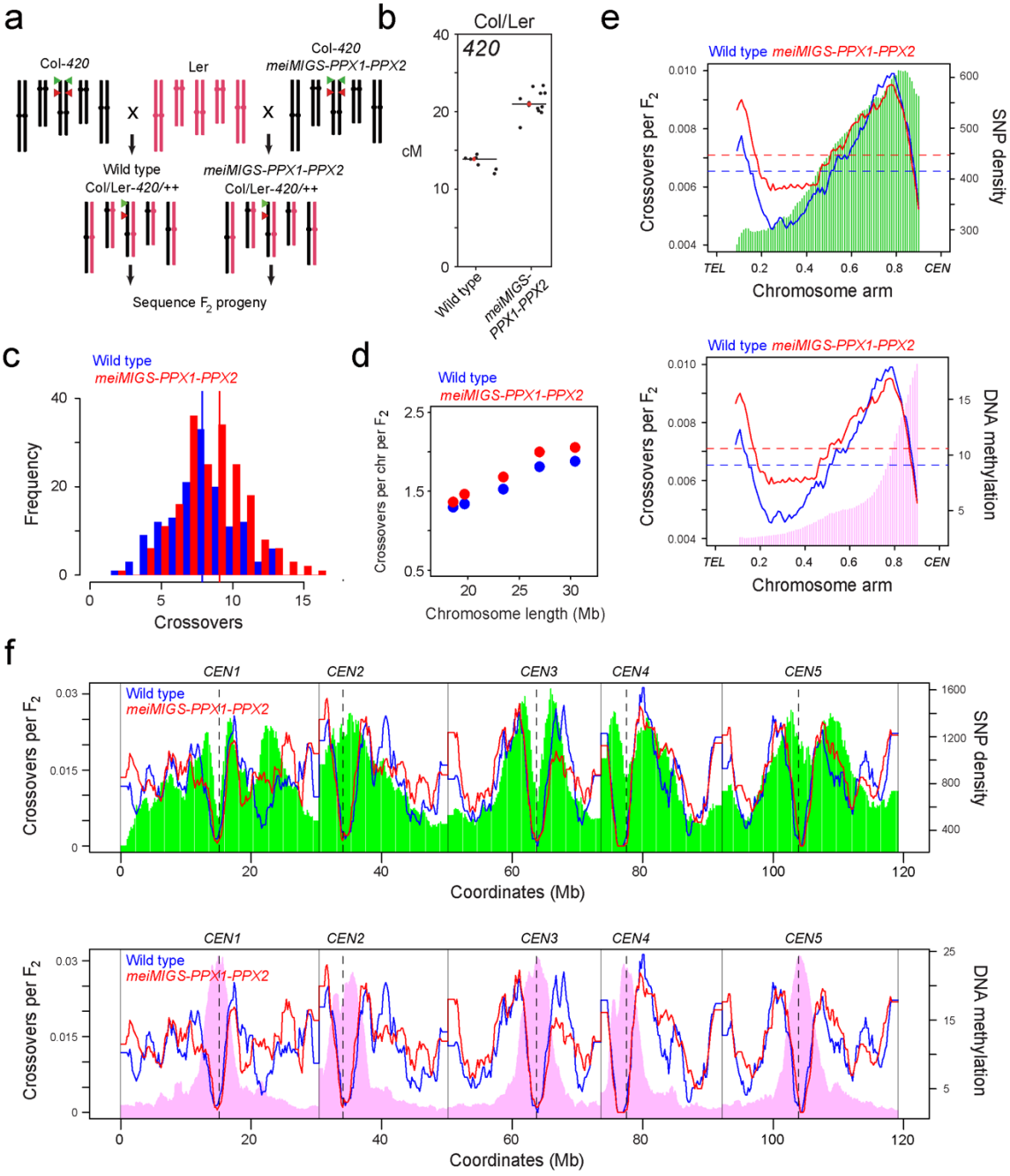

Figure 4. Genome-wide mapping of crossovers in *meiMIGS-PPX1-PPX2*. **a,** Schematic diagram showing crossing of *meiMIGS-PPX1-PPX2* Col-*420* (black) and wild type Col-*420* (black), to Ler (red) to generate F_2 populations for genotyping-by-sequencing. Green and red triangles indicate *420* T-DNAs on chromosome 3. **b,** *420* crossover frequency (cM) in wild type and *meiMIGS-PPX1-PPX2* Col/Ler F_1 hybrids. **c,** Histogram of crossover number per F_2 individual in wild type (blue) Col/Ler and *meiMIGS-PPX1-PPX2* (red) populations. Vertical dashed lines indicate mean values. **d,** Crossovers per chromosome per F_2 compared with chromosome length in wild type (blue) and *meiMIGS-PPX1-PPX2* (red). **e,** Normalized crossover frequency plotted along chromosome arms orientated from telomere (*TEL*) to centromere (*CEN*) in wild type (blue) and *meiMIGS-PPX1-PPX2* (red) F_2 populations. Mean values are indicated by horizontal dashed lines. Also plotted is Col/Ler SNP frequency (green, upper) and DNA methylation (pink, lower). **f,** As for e, but without telomere-centromere scaling. Vertical solid lines indicate telomeres and vertical dotted lines indicate centromeres.

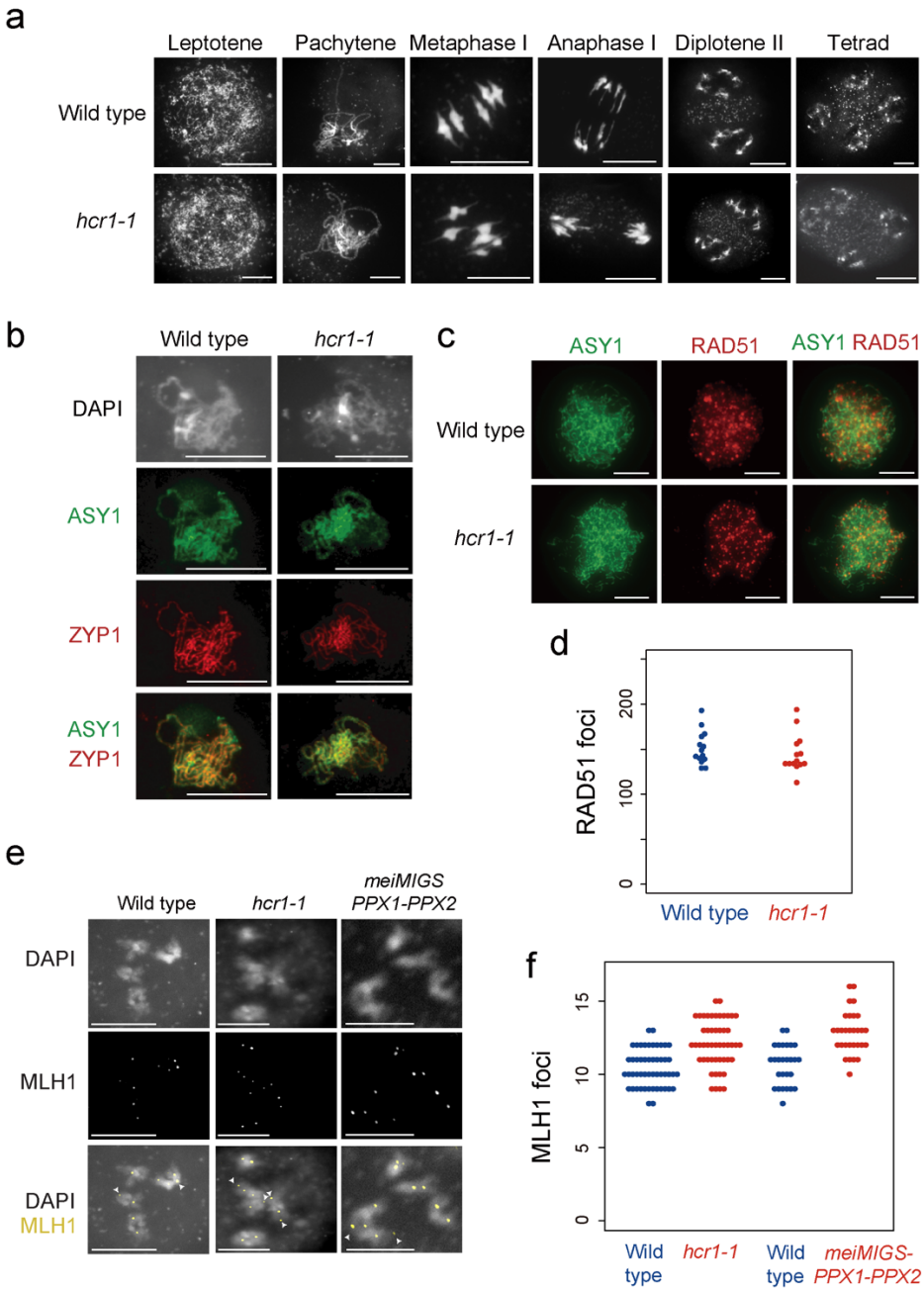

Figure 5. Meiotic MLH1 foci are elevated in *hcr1* whereas RAD51, ASY1 and ZYP1 immunostaining are unchanged. a, Representative images of male meiocytes spread and stained with DAPI in wild type (Col) and *hcr1-1*, at the labeled stages of meiosis. Scale bars=10 µm. **b,** Representative images of ASY1 (green) and ZYP1 (green) immunostaining of wild type (Col-0) and *hcr1-1* male meiocytes at pachytene. Nuclei spreads were also stained with DAPI. Scale bars=10 µM. **c,** Representative images of ASY1 (green) and RAD51 (red) co-immunostaining on wild type (Col-0) and *hcr1-1* male meiocytes during early prophase I. Scale bars=10 µM. **d,** Quantification of RAD51 foci number per cell in wild type and *hcr1-1*. **e,** Representative images of MLH1 (red) immunostaining of male meiocytes at diakinesis stage in wild type, *hcr1-1* and *meiMIGS-PPX1-PPX2*. Cells were also DNA stained with DAPI (blue). Arrows represent MLH1 foci at distal locations on the chromosomes. Scale bars=10 µM. **f,** Quantification of MLH1 foci number per cell scored at diakinesis stage in wild type (blue), *hcr1-1* (red) and *meiMIGS-PPX1-PPX2* (red). Scale bars=10 µM. All cytological experiments represent data collected from at least two biological replicates.

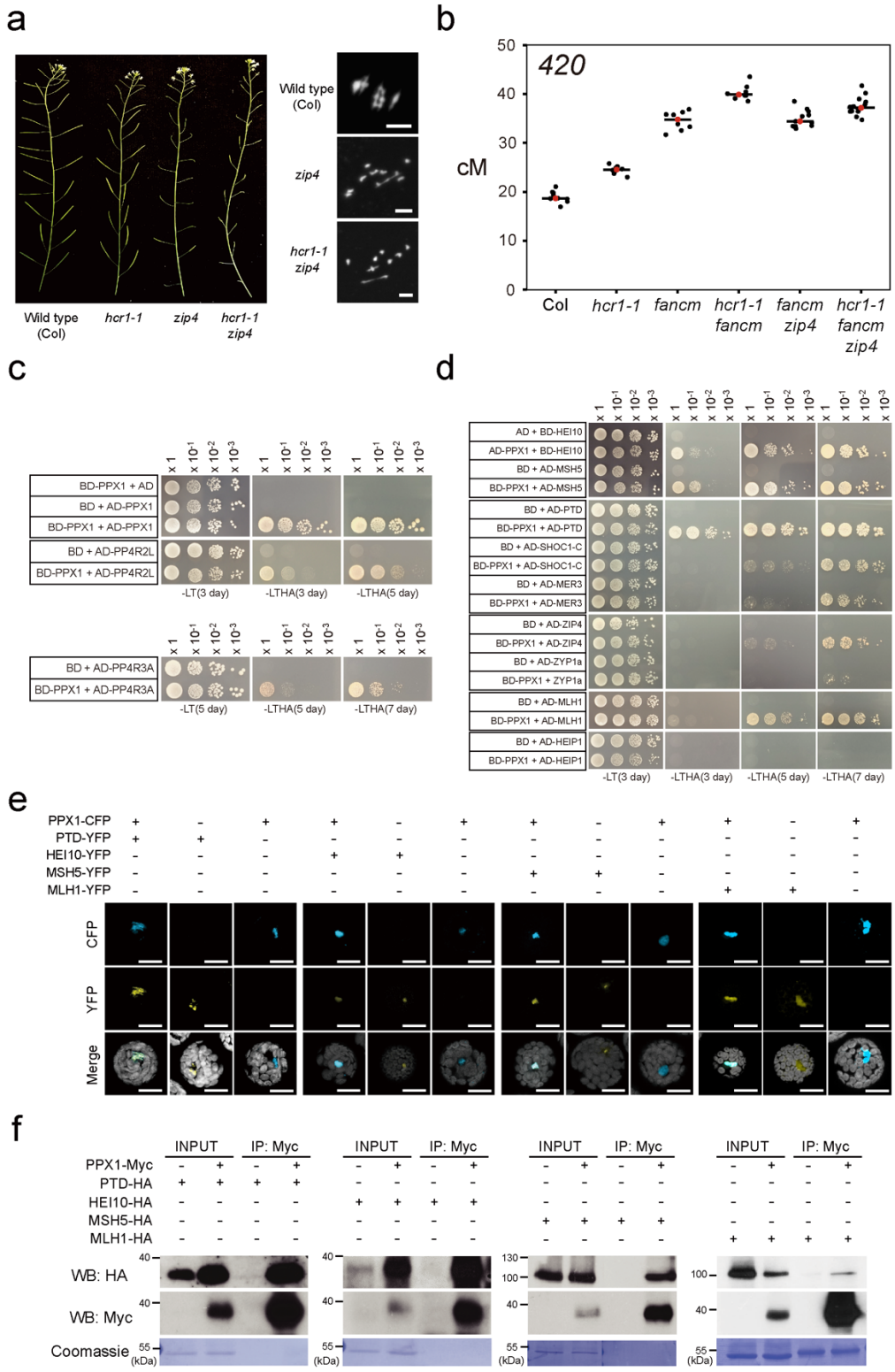

Figure 6. HCR1 genetically and physically interacts with the Class I crossover pathway. **a,** Representative siliques from wild type, *hcr1-1*, *zip4* and *hcr1-1 zip4* plants. Shown alongside are representative metaphase I chromosome spreads stained with DAPI from wild type (Col), *zip4* and *zip4 hcr1*. This was repeated with three biological replicates. Scale bars=10μM. **b,** *420* crossover frequency (cM) in wild type, *hcr1-1*, *fancm*, *fancm zip4*, *hcr1-1 fancm* and *hcr1-1 fancm zip4*. Mean values are indicated by red dots and horizontal lines.

c, Yeast two hybrid assays showing interactions of HCR1 with PP4R2 and PP4R3. Yeast co-transformants were grown until OD_{600}=1, diluted 10-, 100- and 1,000-fold, spotted on synthetic dropout media (SD) lacking leucine/tryptophan (-LT) and leucine/trptophan/histidine/adenine (-LTHA) and grown for 3 to 5 days. **d,** As for c, but showing interactions of HCR1 with HEI10, PTD and MSH5, and weaker interactions with SHOC1, MER3, ZIP4, MLH1 and ZYP1a. Yeast transformants were grown on SD (-LTHA) for 3, 5 or 7 days. **e,** Co-localization of fluorescent protein fusions with HCR1 and HEI10, PTD, MSH5 and MLH1 in Arabidopsis protoplasts. All scale bars=20 μm. Experiments were repeated at least three times. **f,** Coimmunoprecipitation analyses of HCR1 and HEI10, PTD, MSH5 and MLH1. IB=immunoblot; IP=immunoprecipitation. Experiments were repeated at least three times.

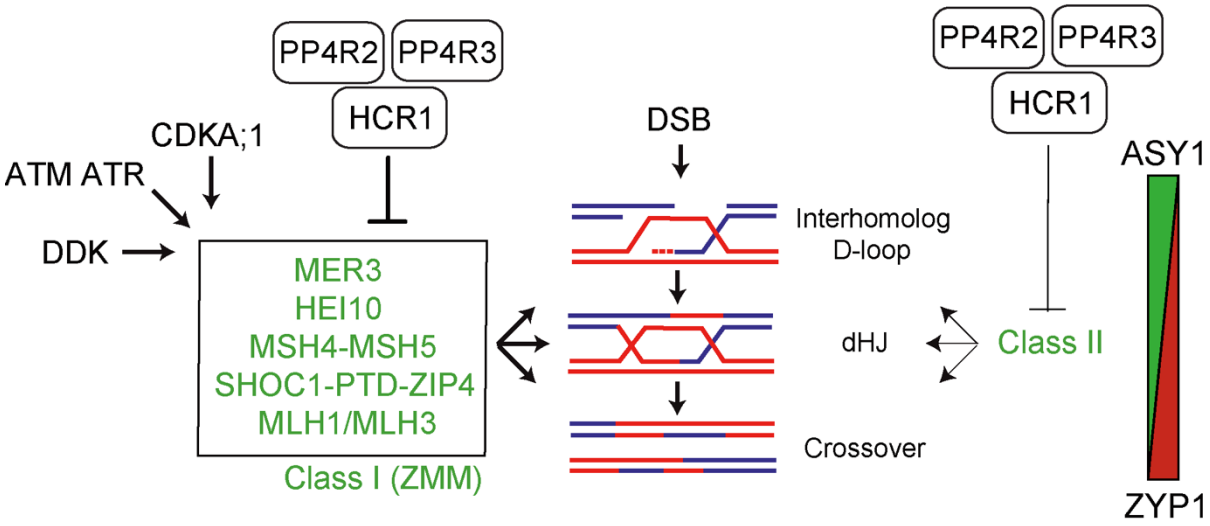

Figure 7. HCR1/PPX1 PP4 control of meiotic crossover recombination in Arabidopsis. During meiosis, recombination is initiated by DNA double strand breaks (DSB) that can be resected to form single stranded DNA (ssDNA). In the central diagram a resected ssDNA end (blue) from one homolog has invaded the second homolog (red), to form an interhomolog displacement loop (D-loop). A subset of IH D-loops are further processed to form double Holliday junctions (dHJs), which may be resolved into a crossover. The Class I (also known as ZMM) pathway proteins (green) acts at multiple steps within the formation and stabilization of IH D-loops and dHJs and their resolution into interfering crossovers. The activity of the Class I pathway has been shown to be promoted by independent kinase pathways, including CDK, DDK and Mec1/Tel1 (ATM/ATR). We propose that HCR1 acts with PP4R2 and PP4R3 in PP4 phosphatase complexes that antagonize one or more of the pro-recombination kinase pathways on Class I targets and thereby restrict the number of interfering crossovers that form per meiosis. The Class II pathway contributes to ~10% of crossovers in wild type. Our data also indicate a minor role for repression of the Class II pathway by HCR1. On the right is a diagram indicating that during progression of meiotic recombination, the abundance of axis protein ASY1 (green) is depleted, as the synaptonemal complex protein ZYP1 (red) increases.

Methods

Plant materials

Arabidopsis plants were grown under controlled conditions of 22°C, 50-60% humidity and 16/8 hour light-dark cycles. Seeds were incubated at 4°C in the dark for 3-4 days in order to stratify germination. Seed-expressed FTL/CTL and pollen-expressed FTL lines were used[29,30]. T-DNA insertion lines in *ppx1* (GK_651B07), *ppx2* (GK_488H09), *pp4r2* (SALK_093051), *zip4-2*[96] (SALK_068052) and the *fancm-1* EMS mutant[37] were provided by Nottingham Arabidopsis Stock Centre. Genotyping of *hcr2-1* was performed by PCR amplification using oligonucleotides ppx1-F and ppx1-R for wild type, and ppx1-F and GABI_LB for the T-DNA allele. Genotyping of *ppx2-1* was carried out by PCR amplification using primers ppx2-F and ppx2-R for wild type, and ppx2-R and GABI_LB for the T-DNA allele. Genotyping of *pp4r2* was performed by PCR amplification using oligonucleotides pp4r2-F and pp4r2-R for wild type, and pp4r2-R and LBb1.3 for the T-DNA allele. Genotyping of *hcr1-1* was performed by PCR amplification using hcr1-F and hcr1-R dCAPs markers, followed by *Fok*I restriction endonuclease digestion. *zip4-2* and *fancm-1* genotyping was performed as previously described[33]. Genotyping oligonucleotide sequences can be found in Supplementary Table 24.

Ethyl-methyl sulfonate mutagenesis of Arabidopsis seed

Approximately 10,000 seeds from *420 GR/++* hemizygote plants were obtained by crossing *420* (*GR/GR*) homozyotes to wild type (Col-0). These seed were soaked in 40 ml of 100 mM phosphate buffer (pH 7.5) in a 50 ml tube for 1 hour. Seeds were washed with fresh 100 mM phosphate buffer and then treated with 0.3% (v/v) ethyl-methyl sulfonate (EMS) and incubated for 12 hours at room temperature. EMS treated seeds were washed 10 times with distilled water and immediately sown on soil. From these seed, ~7,000 M_1 plants were germinated and grown. The seeds from 12 independent M_1 plants were combined to generate ~600 M_2 pools. From each M_2 pool, approximately ~150 seeds were pre-selected as *420/++* hemizygotes, based on red and green fluorescence, grown and self-fertilized. The resulting seed were analysed for *420* crossover frequency.

Measurement of crossover frequency and interference using fluorescent seed and pollen

Crossover frequency was measured by analyzing counts of fluorescent and non-fluorescent seeds from *FTL/++* hemizygote plants using a CellProfiler image analysis pipeline[97,98]. CellProfiler enables the quantification of green-alone fluorescent seeds (N_{Green}), red-alone fluorescent seeds (N_{Red}) and total seeds (N_{Total}). Crossover frequency (cM) is calculated using the formula: $cM = 100\times(1-[1-2(N_{Green}+N_{Red})/N_{Total}]^{1/2})$[30,32]. To test whether crossover frequency was significantly different between genotypes we used Welch's t-tests.

Pollen FTLs were generated in *qrt-1* mutant background, where the four-pollen products of male meiosis are attached to one another[31]. FTLs express eYFP (Y), dsRed (R) or eCFP (C) fluorescent proteins under the post-meiotic *LAT52* promoter. Pollen tetrad FTL-based measurement of crossover frequency and interference were carried out using DeepTetrad, as described[31,55]. DeepTetrad is a deep learning-based image analysis pipeline that recognizes pollen tetrad classes of two or three-color FTL intervals. The two color FTL interval *CEN3* produces parental ditype (PD), tetra type (T), and non-parental ditype (NPD) tetrads, and crossover frequency was calculated using the Perkin's equation:

$$cM = \frac{0.5T + 3NPD}{\left(PD + T + NPD\right)} * 100$$

Three-color FTL intervals (*I1bc, I1fg, I2fg, I3bc* and *I5ab*) produce 12-tetrad classes: no recombination (A), single crossover interval 1 (B; SCO-*i1*), single crossover interval 2 (C; SCO-*i2*), two-strand double crossover (D; 2stDCO), three-strand double crossover a (E; 3st DCOa), three-strand double crossover b (F; 3st DCOb), four-strand double crossover (G; 4st DCO), non-parental ditype interval 1, non-crossover interval 2 (H; NPD-*i1* NCO-*i2*), non-crossover interval 1, non-parental ditype interval 2 (I; NCO-*i1* NPD-*i2*), non-parental ditype interval 1, single crossover interval 2 (J; NPD-*i1* SCO-*i2*), single crossover interval 1, non-parental ditype interval 2 (K; SCO-*i1* NPD-*i2*) and non-parental ditype interval 1, non-parental ditype interval 2 (L; NPD-*i1* NPD-*i2*)[31]. Fluorescent tetrad states were identified using DeepTetrad and crossover frequency (cM) was calculated using the Perkin's equation.

Crossover interference ratio (IFR=σ) in two linked intervals, which is the ratio of the genetic map distance with an adjacent crossover χ_γ to the genetic map distance without an adjacent crossover χ_δ, was calculated by DeepTetrad using the formulae:

$$\chi_\gamma = \frac{0.5T_\gamma + 3NPD_\gamma}{PD_\gamma + T_\gamma + NPD_\gamma} = \frac{0.5(D+E+F+G+K)+3(J+L)}{(C+I)+(D+E+F+G+K)+(J+L)}$$

$$\chi_\delta = \frac{0.5T_\delta + 3NPD_\delta}{PD_\delta + T_\delta + NPD_\delta} = \frac{0.5(B)+3(H)}{(A)+(B)+(H)}$$

$$\sigma = \frac{\chi_\gamma}{\chi_\delta}$$

Identification of candidate *hcr1-1* mutations using DNA sequencing and SHOREmap

Sixty *hcr1* BC_1F_2 individuals with high (>27 cM) *420* crossover frequency were identified and 5 mg of seed from each BC_1F_2 individual were pooled. Sterilized seed were germinated on ½ MS agar plates and bulk 7-day old seedlings collected. ~3 grams of pooled seedlings were ground in liquid N_2 using a mortar and pestle. The leaf powder was transferred into a pre-chilled mortar with 40 ml of fresh nuclear isolation buffer (25 mM Tris-HCl, pH 7.5, 0.44 M sucrose, 10 mM $MgCl_2$, 0.5% Triton X-100, 10 mM β-mercaptoethanol, 2 mM spermine, EDTA-free Protease Inhibitor Cocktail) and the contents were homogenized. The tissue lysate was kept on ice and incubated for 30 minutes with rocking. The filtered contents were centrifuged at 4°C at 3,000*g* for 25 minutes. The supernatant was removed and the pellet was subjected to DNA extraction using CTAB. CTAB-extracted and purified DNA was sheared to a size range 200-500 bp using a Bioruptor sonicator. 1 µg of input DNA was diluted in 150 µl of TE buffer and sonicated for 22 minutes using high voltage with 30 second ON/OFF cycles. The sonicated DNA was concentrated in a 60 µl volume and DNA in the size range ~300-400 bp from a 2% agarose gel stained with 1×SYBR gold using a UV transilluminator. 50 ng of purified DNA in 60 µl volume was used as input for library construction using an Illumina Truseq Nano DNA LT library prep kit. The *hcr1-1* BC_1F_2 library was sequenced using an Illumina Genome Analyser (100 bp paired) Hiseq 2000 instrument.

SHOREmap (v.3.0) was applied to align paired-end reads to the TAIR10 reference genome using the GenomeMapper tool[38]. Raw reads were trimmed according to quality values with a cut-off Phred score of +33 or +64, using the function SHORE *import*. SHORE function *consensus* was used to detect sequence variation between the *hcr1* BC_1F_2 and the TAIR10 reference assembly. Single nucleotide polymorphisms (SNPs) with high quality marker scores (>40), supported by at least 10 unique reads, were applied using SHOREmap *backcross* for analysis of allele frequency. Using SHOREmap *annotate* we compared the TAIR10 gene annotation and obtained a list of EMS-derived that included predicted effects on gene expression and function. Mutations were screened for those with (i) greater than 80% allele frequency, and (ii) non-synonymous, splice site or premature stop codon changes in predicted

genes. Additionally, candidate mutations were examined based on their location within genes with predicted or known functions relevant to meiosis, protein location in the nucleus, and known molecular functions provided in the TAIR database.

Genetic complementation of *hcr1-1* by *PPX1*

A 4.5 kb genomic DNA fragment containing *HCR1*/*PPX1* was PCR amplified using primers PPX1-F and PPX1-R (Supplementary Table 24). The PCR product was digested by *Pst*I and *Sma*I restriction enzymes and cloned into the binary vector pGREEN0029. The pGREEN0029-*PPX1* and empty vector constructs were electroporated into *Agrobacterium* strain GV3101-pSOUP and transformed into Arabidopsis plants by floral dipping[99]. T_1 plants were selected for kanamycin resistance and genotyped using primers designed from left and right borders of the *HCR1/PPX1* transgene (Supplementary Table 24).

Construction of PPX/PP4 phylogenetic tree

The neighbour-joining method was used to construct a PPX/PP4 phylogenetic tree. Amino acid sequences of AtPPX1 (NP_194402.1), AtPPX2 (NP_200337.1), OsPPX (XP_015612628), DmPp4-19C (NP_001285489), HsPPP4C (NP_001290432), Cepph-4.1 (NP_499603), Cepph-4.2 (NP_001022898), and ScPPH3 (AJV04101) were used for multiple sequence alignments.

Generation of *meiMIGS-PPX1, meiMIGS-PPX2* and *meiMIGS-PPX1-PPX2* transgenic plants

To generate meiosis-specific microRNA mediated gene silencing (*meiMIGS*) transgenic plants, 1.5 kb of genomic DNA including the *DMC1* promoter, 5´-UTR, two introns and the third exon were PCR amplified from Col genomic DNA using primers DMC1-1p_1.5kb-Lv0-GGAG-F and DMC1-1p_1.5kb-Lv0-CATT-R (Supplementary Table 24). PCR products was cloned into the universal Level 0 (Lv0) vector (pAGM9121) using the Golden Gate cloning system. *PPX1* and *PPX2* cDNA regions were cloned into the Lv0 vector (pAGM9121) following amplification using forward primers that included the miR173 target sequence and reverse primers (Supplementary Table 21). *PPX1-PPX2* fusion cDNA was generated by overlap PCR and cloning into Lv0 vector pAGM9121. The *DMC1* promoter and *MIGS-PPX1/2/1-2* Lv0 vectors were assembled into Lv1 position 2 vector pICH47742 with the *NOPALINE SYNTHASE GENE (NOS)* terminator (pICH41421). Each Lv1 vector containing meiMIGS cassettes was assembled into a Level 2 (Lv2) binary vector (pAGM4723) with the antibiotic resistant gene *BAR* containing Lv vector (pICSL11017) and linker (pICH41744). The Lv2 binary vectors were electroporated into Agrobacterium strain GV3101-pSOUP and transformed into Arabidopsis by floral dipping.

Genotyping-by-sequencing of F_2 plants and crossover identification

Genomic DNA from wild type and *meiMIGS-PPX1-PPX2* Col/Ler F_2 individuals was extracted using CTAB to prepare sequencing libraries, as described[56]. 150 ng of DNA was fragmented using 0.3 units of dsDNA Shearase (Zymo Research) in a final volume of 15 µl. The digested DNA was end-repaired for 30 minutes at 20°C in a reaction volume of 30 µl (3 units of T4 DNA polymerase (New England Biolabs), 10 units of T4 polynucleotide kinase (Thermo Fisher Scientific), 1.25 units of Klenow fragment (New England Biolabs) and 0.4 mM dNTPs). DNA fragments were cleaned using AMPure XP magnetic SPRI beads (Beckman-Coulter, A63881), as described[56]. DNA was A-tailed, and then ligated with barcoded Illumina adaptors in a reaction volume of 20 µl, as described[56]. Eight DNA libraries were pooled, washed and eluted in 30 µl elution buffer (10 mM Tris-HCl, pH 8.0). The 30 µl mixture was combined in a tube containing 16 µl of AMPure XP magnetic SPRI beads (Beckman-Coulter). After 5 minutes of

incubation at room temperature, the samples were placed in a magnetic rack for 2 minutes and the supernatant (42 µl) was transferred to a fresh tube and mixed with 0.23 volumes (9.5 µl) of SPRI beads. After 5 minutes of incubation at room temperature, the tubes were placed on a magnetic rack for 2 minutes. The supernatant was discarded, and the beads washed twice with 80% ethanol for 30 seconds. The beads were air-dried for 10 minutes and DNA was eluted in 20 µl of 10 mM Tris (pH 8.0). 12 µl of the eluate was amplified using twelve cycles of PCR in a reaction volume of 50 µl using KAPA HiFi Hot-Start ReadyMix PCR kit (Kapabiosystems) and the reported DNA oligonucleotides[56]. The PCR products were then purified using SPRI beads and quantified using a Bioanalyzer. The 96 barcoded libraries were subjected to paired-end 150 bp sequencing using an Illumina HiSeqX instrument.

Immunocytological analysis of wild type and *hcr1* meiocytes

Chromosome spreads of Arabidopsis pollen mother cells was prepared using fixed buds and DAPI-stained, as described[100]. Pachytene cells were immunostained for ASY1 and ZYP1, and diakinesis cells were immunostained for MLH1, using fixed buds, as described[100,101]. Leptotene-stage meiocytes were immunostained for ASY1 and RAD51 using fresh buds, as described[102]. The following antibodies were used: α-ASY1 (rat, 1:200 or 1:500 dilution), α-ZYP1 (rabbit, 1:200 dilution), α-MLH1 (rabbit, 1:200 dilution) and α-RAD51 (rabbit, 1:300 dilution)[100,102,103]. Microscopy was performed using a DeltaVision personal DV microscope (Applied precision/GE Healthcare) equipped with a CDD Coolsnap HQ2 camera (Photometrics). Image capture was carried out using SoftWoRx software version 5.5 (Applied precision/GE Healthcare). For ASY1 and RAD51 co-immunostaining of leptotene-stage nuclei, individual cell images were acquired as *Z*-stacks of 10 optical sections of 0.2 µM each, and the maximum intensity projection for each cell was decided using ImageJ. Number of MLH1 foci per meiotic cell and RAD51 foci per cell associated with the axis protein ASY1 were manually scored. Wilcoxon tests were used to assess significant differences between wild type and *hcr1-1* MLH1 and RAD51 foci counts.

Yeast two hybrid assays

For yeast two-hybrid (Y2H) assays the open reading frames of Arabidopsis genes were cloned into pGBKT7 BD and pGADT7 AD vectors (Clontech, 630490) using *Bam*HI and *Stu*I sites, using a Gibson assembly cloning system (NEB #E2621L). Information of all oligonucleotides used for Y2H assays are in Supplementary Table 24. Both BD and AD vectors were co-transformed into *S. cerevisiae* strain AH109 and selected on synthetic dropout medium lacking leucine (-L) and tryptophan (-T). The colonies of yeast transformant cells were streaked onto both (-LT) and (-LTH (histidine) A (adenine)) synthetic mediums and grown for 3 to 5 days at 30°C. The cells grown in synthetic medium (-LT) were grown until OD_{600} = 1 and diluted 10-, 100- and 1,000-fold in water and spotted on synthetic medium (-LTHA) for 3 to 7 days.

Transient expression of fusion proteins in Arabidopsis protoplasts for co-localization and co-immunoprecipitation analysis

Transient expression vectors in protoplasts were constructed using Golden Gate cloning. The full-length coding regions of *PPX1/HCR1* and meiotic genes were PCR amplified from cDNA and cloned into Lv0 universal vector (pICH41331). For epitope and fluorescent protein tagging, the Lv0 vectors with coding regions lacking stop codon were assembled in the Lv1 transient expression vector (pICH47742), using the *35S* promoter vector (pICH51266), C-terminal vectors (YFP, CFP, Myc tag/pICSL50010 and HA tag/pICSL50009) and *NOPALINE SYNTHASE GENE* (*NOS*) terminator vector (pICH41421). Information of all oligonucleotides for protoplast transient expression is provided in Supplementary Table 24.

Plasmid DNA and mesophyll protoplasts were prepared, as described[104]. 20×10^3 protoplasts were transfected with 20 µg of total plasmid DNA and incubated for 6-12 hours at room temperature. To detect colocalization of PPX1-CFP and meiotic protein-YFP, 20 µg of total plasmid DNA (a mixture of *PPX1-CFP* with *YFP* fusion constructs *HEI10-YFP, PTD-YFP* or *MSH5-YFP*) were co-transfected into 20×10^3 protoplasts and incubated at room temperature for 12 hours. As a negative control, *PPX1-CFP* alone or *YFP*-fusion plasmid alone were transfected. The fluorescence of transfected mesophyll protoplasts was detected using a confocal microscope (LSM 800, Zeiss).

For co-immunoprecipitation analysis, 40 µg of *PPX1*-Myc tag and meiotic gene-HA tag DNA plasmids were co-transfected into protoplasts, or individually transfected as a negative control. Total protein was extracted using extraction buffer (50 mM Tris-HCl pH 7.5, 100 mM NaCl, 5 mM EDTA, 1 mM dithiothreitol, protease inhibitor cocktail (Roche) and 1% Triton X-100). The extracted proteins were separated by SDS–PAGE using 8% polyacrylamide gels, transferred to a nitrocellulose membrane and immunodetected with anti-HA (1:2,000 Roche 12013819001) or anti-Myc (1:2,000 Santa Cruz sc-9E10) antibodies. For co-immunoprecipitation (Co-IP) analysis, transfected protoplasts were lysed with IP buffer (50 mM Tris-HCl pH 7.5, 100 mM NaCl, 1 mM EDTA, 0.5% Triton X-100, 10% glycerol and protease inhibitor cocktail). Lysates were incubated with 1 µg anti-myc antibody for 12 hours with rotation at 4 °C. Then, the protoplast lysate and antibody mixture were incubated with 50% protein G-coated agarose beads (Millipore 16-201), pre-cleared with IP buffer, for an additional 2 hours. Protein-coated agarose beads were washed with IP buffer three times. Proteins were extracted using extraction buffer and subjected to western blotting using anti-HA antibodies.

Prediction of PP4 complex target proteins in Arabidopsis

To predict PP4 target proteins during meiosis, FxxP motif containing proteins were identified by searching protein sequences from TAIR. Nuclear proteins were obtained from the TAIR10 GO cellular compartment annotation by selecting terms "nucleus", "other cellular components: host cell nucleus", "other cellular components: nucleus-vacuole junction". We used a previous RNA-seq dataset, which identified genes that showed significantly higher expression in male meiocytes compared to leaf[34]. The meiotically expressed, nuclear proteins with FxxP motifs were further classified according to the presence of predicted phosphorylation consensus sites of CDK, DDK and ATM/ATR, predicted using GPS 5.0[105]. To test for significant enrichment of phosphorylation consensus motifs in the predicted PP4 target proteins, we generated random sets of the same number of genes which were analysed for predicted phosphosites. The observed phosphosite overlaps were compared with the random using a Z-test.

Data Availability

Genome sequencing data of F_2 plants can be found at the ArrayExpress repository hosted by the European Bioinformatics Institute (EBI) (https://www.ebi.ac.uk/arrayexpress/). The data can be found at accessions E-MTAB-9621 and E-MTAB-10168.

Extended Data Figure Legends

Extended Data Fig. 1. *420* crossover frequency in wild type and M_2 plants derived from the EMS population. Box and whisker plot showing *420* crossover frequency (cM) for wild type (Col/Col) *420/*++ plants (n=75) and EMS-treated M_2 *420/*++ plants (n=1,217). Black dots indicate 420 crossover frequency in individual plants. Horizontal lines of black (wild type, Col) and red (EMS M_2) box plots represent maximum, 3rd quartile, median, 1st quartile and minimum in *420* cM. In this study, wild type plants show a mean value of 19.5 cM (standard deviation=1.5) within *420*, and the majority (81.4%, 991/1,217) of M_2 plants display *420* crossover frequency within the range of 18-22 cM (Mean=21.4 cM, SD=1.5). *420* crossover frequency in M_2 plants was significantly increased compared to wild type (Welch's t-test $P=2.2\times10^{-16}$), which may have been caused by heterozygous EMS polymorphisms.

Extended Data Fig. 2. EMS mutations identified in *FANCM* (*hcr4*) and *TAF4b* (*lcr1*) a, *FANCM* gene structure is shown, including the EMS mutation site in *hcr4/fancm-11*. The red arrow indicates the G to A substitution within exon 15, which causes a G to S amino acid substitution. Exons are shown as boxes (black=CDS, grey=UTR). Scale bar=0.5 kb. **b,** Multiple sequence alignment of the DEHDc (blue line) and HELICC (green line) domains of FANCM in different species. The mutation positions of the *fancm-1* to *fancm-10* alleles that were previously identified[1,2], and *fancm-11* (*hcr4*), are shown. The *fancm-11* mutation is located in a conserved motif within the SF2 helicase domain (bold arrow). **c,** Gene structure of *TAF4b* is shown with the location of the *lcr1* (*taf4b-3*) mutation indicated in exon 3 (red arrow), which causes a premature stop codon.

Extended Data Fig. 3. T-DNA insertions in Arabidopsis *PP4/PPX* complex genes. a, The gene structures of *PPX1* (At4g26720), *PPX2* (At5g55260) and *PP4R2* (At5g17070) are shown. Exons are shown as boxes (black=CDS, grey=UTR). Scale bar=0.5 kb. The EMS induced *hcr1-1* mutation is located at the splice donor site of the 3rd intron, shown by the asterisk. The red arrows indicate the location of primers for RT-qPCR in *PPX1* and *PPX2*. The *hcr1-2* T-DNA (GK_651B07) insertion position in the 5´-UTR is indicated. The position of the *ppx2-1* (GK_488H09), *ppx2-2* (SALK_049725), and *pp4r2* (SALK_093051) T-DNA insertions are shown, which are located in the 4th intron, 8th exon and 7th intron, respectively. The arrows spanning the *ppx2* and *pp4r2* T-DNA insertions indicate primer positions used for RT-PCR. **b,** RT-PCR amplification and quantification for *PPX1, PPX2* and *PP4R2* mRNA expression in wild type Col, *hcr1-1*, *ppx1-2*, *ppx2-1* and *pp4r2*. Floral cDNA from two biological replicates were evaluated by RT-PCR amplification for *PPX1*, *PPX2*, *PP4R2* (shown in a) and *GAPC* expression. RT-PCR amplicon sizes for wild type, *hcr1-1*, *ppx1-2*, *ppx2-1*, *pp4r2* cDNAs and wild type genomic DNA (positive/negative control) are shown. **c**, Plot showing RT-qPCR enrichment of *PPX1* and *PPX2* in *hcr1-1* and *ppx2-1*. Relative transcript levels of *PPX1* and *PPX2* were measured in wild type, *hcr1-1*, and *ppx2-1* using qRT-PCR. *TUB2* was used for normalization. The y axis indicates fold-enrichment of *PPX1* and *PPX2* transcript levels, compared to *PPX1* and *PPX2* in wild type. RT-qPCR reactions of two technical replicates for each of four biological samples were shown as dots. Mean values are indicated by horizontal lines. Significance between wild type and mutants was assessed by Welch's t-test. Asterisks indicate $P<0.001$. **d,** Photograph showing developmental phenotypes of wild type, *hcr1-2*, *hcr1-1*, *ppx2-1*, *hcr1-2 ppx2-1* and *hcr1-1 ppx2-1* grown alongside one another. **e,** Photograph showing seeds of wild type and *hcr1-1/+ ppx2-2/+* plants. Asterisks indicate defective seeds. **f,** Photograph showing F_2 seedlings grown from self-fertilization of F_1 *hcr1-1/+ ppx2-2/+* plants, with asterisks indicating developmentally delayed seedlings.

Extended Data Fig. 4. Alignment of PP4 homolog protein sequences from diverse eukaryotes. a, Amino acid sequence alignment of AtPPX1, the predicted *hcr1-1* truncated protein, AtPPX2 and PP4 homologs from different eukaryotic species. The predicted *hcr1-1*

truncated protein consisting of 143 residues is shown. The underlined region indicates amino acids generated due to the retention of the 3rd intron. Hash symbols indicate the locations of conserved PP4 catalytic motifs (GDXHG, GDXVDRG and GNHE) and the histidine (H) residues required for metal binding in C-terminal region. **b,** As for a, but showing percent identity of amino acid sequence between PP4 homologs.

Extended Data Fig. 5. Meiosis-specific knockdown of *PPX1* and *PPX2* in *meiMIGS* transgenic plants. a, qRT-PCR analysis of *PPX1/HCR1* and *PPX2* transcripts in floral buds of wild type and *meiMIGS-PPX1*, *meiMIGS-PPX2* and *meiMIGS-PPX1-PPX2* T_2 transgenic lines. The y axis indicates fold-enrichment of *PPX1* and *PPX2* transcripts, compared to *PPX1* in wild type. *DMC1* was used as a meiotic gene for normalization. Replicate measurements are shown as dots and mean values shown by horizontal lines. **b,** Correlation between *PPX1* and *PPX2* transcript levels in wild type, *meiMIGS-PPX1*, *meiMIGS-PPX2*, and *meiMIGS-PPX1-PPX2* lines. The x and y axis indicate relative *PPX1* and *PPX2* transcript levels in *meiMIGS-PPX1* (blue), *meiMIGS-PPX2* (red), and *meiMIGS-PPX1-PPX2* (green) lines respectively, compared to *PPX1* and *PPX2* expressions in wild type Col plant (r=0.80, P value=1.21×10^{-5}).

Extended Data Fig. 6. Crossover frequency and interference measured in wild type and *hcr1-1* using fluorescent pollen. **a,** Crossover frequency measured using the pollen FTLs *I1bc* and *I3bc* from wild type and *hcr1-1*. Crossover frequency in each interval of the three-color FTLs was measured using the DeepTetrad pipeline[3] (Supplementary Table 20). **b,** Crossover interference ratio measured using FTL pollen tetrads in wild type and *hcr1-1*. Crossover interference ratio (IFR) were calculated using the DeepTetrad pipeline[3,4]. **c,** Plots showing the % of tetrads containing double crossovers, using data from the three-color FTL intervals in wild type and *hcr1-1*. **d,** As for c, but showing FTL data from the *I1bc, I1fg, I3bc* and *I5ab* intervals in wild type and *meiMIGS-PPX1-PPX2*. Tetrads were classified into 12 fluorescence classes (A-L) by DeepTetrad, as described[3,4]. Mean values are indicated by horizontal lines.

Extended Data Fig. 7. SPO11-1-oligonucleotides and nucleosome occupancy around wild type and *meiMIGS-PPX1-PPX2* crossovers. 10 kb windows surrounding crossover midpoints identified from wild type or *meiMIGS-PPX1-PPX2* plants, or the same number of randomly selected positions, were analysed for SPO11-1-oligos ($\log_2$(SPO11-1-oligos/gDNA), red) or nucleosome occupancy ($\log_2$(MNase-seq/gDNA), blue)[5].

Extended Data Fig. 8. Yeast two hybrid assays showing interactions of HCR1/PPX1 with meiotic proteins. a, Yeast two hybrid assays testing interaction between HCR1/PPX1 and Class I (ZMM) proteins. The yeast co-transformants were grown until OD_{600} = 1 and spotted on synthetic dropout media (SD) lacking leucine/tryptophan (-LT) and leucine/trptophan/histidine/adenine (-LTHA) for 3, 5 or 7 days. **b,** Yeast two hybrid assays of HCR1/PPX1 and meiotic proteins involved in axis formation, DSB formation and DNA repair. The yeast transformants were grown until OD_{600} = 1, then diluted 10-, 100- and 1,000-fold in water, and spotted on SD (-LT) and SD (-LTHA) plates to examine growth in 3, 5, or 7 days (Supplementary Table 23).

Extended Data Fig. 9. The EVH1 domain of Arabidopsis PP4R3A interacts with meiotic proteins. a, Yeast two-hybrid assays testing interaction between the PP4R3A EVH1 domain and meiotic proteins. PP4R3A-N indicates the PP4R3A N-terminal region (1-166 aa) containing the EVH1 domain. The yeast co-transformants were grown until OD_{600} = 1 and spotted on synthetic dropout media (SD) lacking leucine/tryptophan (-LT) and leucine/trptophan/histidine/adenine (-LTHA) for 3 and 5 days. The yeast transformants were grown until OD_{600} = 1, then diluted 10-, 100- and 1,000-fold in water, and spotted on SD (-LT)

and SD (-LTHA) plates to examine growth. **b,** Venn diagram summarizing yeast two hybrid assays of meiotic proteins that interact with HCR1/PPX1 and the PP4R3A EVH1 domain. **c,** A schematic model of Arabidopsis PP4 holoenzyme complex that recognizes target protein HEI10 for dephosphorylation via the PP4R3A EVH1 domain and PPX1.

Extended Data Fig. 10. **Genome-wide prediction of PP4 complex target proteins during meiosis. a,** Protein domain (green) structure of Arabidopsis PP4 subunits PPX1, PPX2, PP4R2 and PP4R3. **b,** Amino acid alignment of the PP4R3A homolog EVH1 domain (red box). Hash symbols (#) indicate conserved tyrosine (Y) and tryptophan (W) residues. **c**, As for a, but showing the positions of FxxP motifs and phosphorylation consensus sites in PTD, HEI10, MSH5 and MLH1. **d,** Venn diagram showing overlap of meiotically expressed, nuclear proteins with FxxP motifs. **e,** Venn diagram showing overlap of candidate PP4 target proteins with CDK, DDK or ATM/ATR kinase consensus motifs, predicted using GPS 5.0[6]. The location of HCR1 Y2H interactors are indicated within the Venn diagram. **f,** Histogram showing a significant enrichment of proteins containing phosphorylation sites in the predicted 1,367 PP4 targets, compared to 1,000 sets of randomly chosen genes (n=1,367). The vertical red line indicates observed predicted PP4 target proteins containing phosphorylation sites, compared to the random sets (black lines). **g,** Gene ontology (GO) enrichment analysis of the predicted PP4 targets, using PANTHER (http://pantherdb.org/). Benjamini-Hochberg False Discovery Rate (FDR) correction was used for enrichment test.